

Doubly nonlinear superconducting qubit

Dat Thanh Le,^{1,2,*} Arne Grimsmo,³ Clemens Müller,^{1,4} and T. M. Stace^{1,†}

¹*ARC Centre for Engineered Quantum System, Department of Physics,
University of Queensland, Brisbane, QLD 4072, Australia*

²*Thang Long Institute of Mathematics and Applied Sciences (TIMAS),
Thang Long University, Nghiem Xuan Yem, Hoang Mai, Hanoi 10000, Vietnam*

³*ARC Centre for Engineered Quantum Systems, School of Physics,
The University of Sydney, Sydney, NSW 2006, Australia*

⁴*IBM Research Zurich, 8803 Rüschlikon, Switzerland*

We describe a superconducting circuit consisting of a Josephson junction in parallel with a quantum phase slip wire, which implements a Hamiltonian that is periodic in both charge and flux. This Hamiltonian is exactly diagonalisable in a double-Bloch band, and the eigenstates are shown to be code states of the Gottesman-Kitaev-Preskill quantum error correcting code. The eigenspectrum has several critical points, where the linear sensitivity to external charge and flux noise vanishes. The states at these critical points thus hold promise as qubit states that are insensitive to common external noise sources.

I. INTRODUCTION

Quantum devices are typically sensitive to noise, which presents the major challenge in developing robust quantum technologies. In contrast, digital technologies rest on the existence of stable states of matter that retain classical information over long times. Fundamentally, this is because stable classical states of matter embody an error correcting code. For example, ferromagnet domains in hard disks energetically implement a repetition code amongst many coupled electronic spins. By analogy, it is desirable to engineer quantum systems whose Hamiltonians encode a quantum error correcting code.

One approach to developing robust quantum devices is to design a ‘symmetry protected’ logical space of nearly degenerate ground states $\{|\bar{0}\rangle, |\bar{1}\rangle\}$ [1], such as the proposed $0-\pi$ qubit [2–6], which rejects charge and flux noise. Here we instead introduce and analyse a simple superconducting circuit with a set of eigenstates that are robust against noise, without relying on ground state degeneracy. This device is built from a Josephson junction (JJ) [7] and a quantum phase slip (QPS) wire [8–11], making its Hamiltonian periodic in both charge and flux. The two junctions in this circuit are dual to each other, by which we name the device the dualmon. We show that the dualmon Hamiltonian is exactly diagonalisable, where there are two quantum numbers each associated to one canonical coordinate, and that typical noise processes commute with the Hamiltonian, affording some symmetry protection to the device.

The energy eigenbasis of the dualmon circuit includes the codewords of the Gottesman-Kitaev-Preskill (GKP) error correcting code [12, 13] which occur at four critical points in the eigenspectrum: one minimum (ground state), one maximum, and two saddle points. At these

critical points, we find that the device is insensitive (at linear order) to fluctuations in both charge and flux, making the critical points promising candidates for robust quantum information storage. We also show that these results hold when the circuit includes realistic parasitic inductance and capacitance.

The paper is structured as follows. In Sec. II, we analyse the characteristics of the elementary dualmon circuit and its robustness to classical noise. Section III takes into account the effect of wire inductance and junction capacitance, which are always present in a realistic circuit. We compute the energy bands of this circuit both analytically and numerically to assess the influence of external flux and charge noise. We also discuss on other possible noise sources in the realistic dualmon circuit. In Sec. IV, we couple the circuit to a waveguide to implement spectroscopy. The resulting transmission spectrum shows that the interband transition is dependent upon the system state, based on which we propose a means for state initialisation. The waveguide coupling additionally gives rise to a quantum noise model; however, it is found that the dualmon remains resilient against the induced quantum noise. Afterwards, in Sec. V we compare the dualmon with several previously investigated superconducting qubit designs. We conclude the paper in Sec. VI. Several appendices are attached providing details of calculations described in the main text.

II. THE ELEMENTARY CIRCUIT

Figure 1a illustrates the elementary dualmon circuit in which an ideal QPS is in parallel with an ideal JJ, so that there is no parasitic capacitance or inductance. The QPS and JJ are dual circuit elements, with constitutive relations $V_Q = V_c \sin(2\pi Q/(2e))$ and $I_J = I_c \sin(2\pi\Phi/\Phi_0)$ respectively, where V_Q is the QPS voltage which depends on the charge, Q , that has flowed through the QPS, I_J is the JJ current which depends on the flux, Φ , linked by the JJ, and $\Phi_0 = h/(2e)$ is the magnetic flux quantum.

* thanhdat.le@uq.net.au

† stace@physics.uq.edu.au

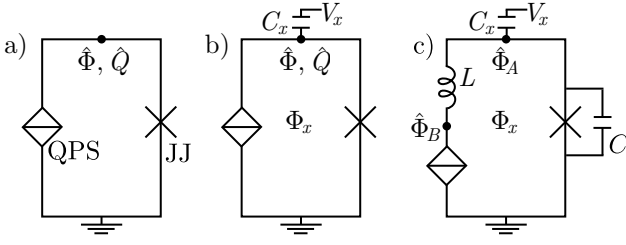


FIG. 1. (a) The elementary dualmon circuit of a quantum phase slip (QPS) wire in parallel with a Josephson junction (JJ). (b) Including coupling to external flux Φ_x and voltage bias V_x . (c) The realistic dualmon circuit including self-inductance L , and parasitic capacitance C .

The QPS and JJ elements are characterised by their critical voltage V_c and critical current I_c respectively.

The quantised circuit is described by the flux $\hat{\Phi}$ and the conjugate charge \hat{Q} . The Hamiltonian for the system is given by

$$\hat{H} = -E_Q \cos(2\pi\hat{n}) - E_J \cos(\hat{\phi}), \quad (1)$$

where $\hat{n} = \hat{Q}/(2e)$ and $\hat{\phi} = 2\pi\hat{\Phi}/\Phi_0$ satisfy $[\hat{\phi}, \hat{n}] = i$, $E_Q = 2eV_c/(2\pi)$, and $E_J = \Phi_0 I_c/(2\pi)$. The Hamiltonian is periodic in both charge and flux, and since $[e^{\pm i\hat{\phi}}, e^{\pm i2\pi\hat{n}}] = 0$, we find that $[\cos(2\pi\hat{n}), \cos(\hat{\phi})] = 0$. The eigenstates of the system $|k, \varphi\rangle$ are therefore characterised by Bloch quantum numbers $k \in (-1/2, 1/2]$ and $\varphi \in (-\pi, \pi]$, and satisfy dual Bloch relations $\langle k, \varphi | \phi + 2\pi \rangle_{\bar{\phi}} = e^{i2\pi k} \langle k, \varphi | \phi \rangle_{\bar{\phi}}$ [14] and $\langle k, \varphi | n + 1 \rangle_{\bar{n}} = e^{i\varphi} \langle k, \varphi | n \rangle_{\bar{n}}$, where the subscripts $\bar{\phi}$ and \bar{n} distinguish the phase and number bases respectively. The basis $\{|k, \varphi\rangle\}$ was introduced and analysed in the work by Zak [15]; we will subsequently call it the Zak basis.

The eigenenergies of \hat{H} are

$$E_{k,\varphi} = -E_Q \cos(2\pi k) - E_J \cos(\varphi). \quad (2)$$

This spectrum, as shown in Figs. 2a and 2b, has four critical eigenstates

$$\{|0, 0\rangle, |0, \pi\rangle, |1/2, 0\rangle, |1/2, \pi\rangle\},$$

where $\nabla E_{k,\varphi} = (\partial_k E_{k,\varphi}, \partial_\varphi E_{k,\varphi}) = 0$, which are the ground state, two saddle points, and the maximally excited state respectively. Notably, the saddle points can be made degenerate when $E_Q = E_J$. We will show that the sensitivity to charge and flux noise vanishes at these critical points to linear order.

Expanding the eigenstates in the phase or number bases

$$|k, \varphi\rangle = \sum_{j=-\infty}^{\infty} e^{i2\pi j k} |\varphi - 2\pi j\rangle_{\bar{\phi}} = \frac{e^{ik\varphi}}{\sqrt{2\pi}} \sum_{j=-\infty}^{\infty} e^{-ij\varphi} |j - k\rangle_{\bar{n}}, \quad (3)$$

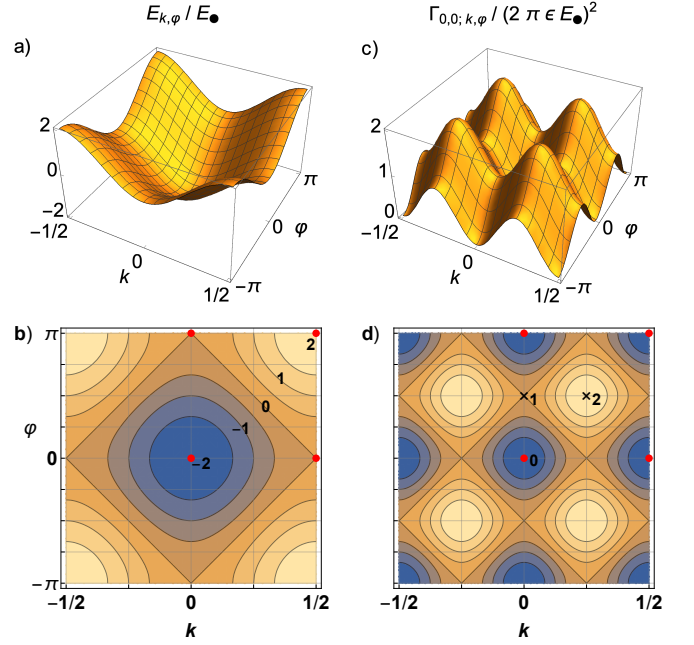


FIG. 2. (a) and (b) Three-dimensional and contour plots of the elementary dualmon circuit energy spectrum, $E_{k,\varphi}$, Eq. (2). The four critical points, where the gradient vanishes, are indicated by red circles. The saddle points are only degenerate if $E_Q = E_J$, but the locations of the critical points are fixed. (c) and (d) The pure dephasing rate $\Gamma_{0,0;k,\varphi}$ of superpositions of the dualmon ground state $|0, 0\rangle$ with other eigenstates $|k, \varphi\rangle$, Eq. (11), due to fluctuations in both external bias charge and flux. The dephasing rate vanishes at the critical points $|k, \varphi\rangle \in \{|0, \pi\rangle, |1/2, 0\rangle, |1/2, \pi\rangle\}$. For illustrative purpose, we have chosen $E_Q = E_J \equiv E_\bullet$ and uniform noise $\epsilon_n = \epsilon_\phi \equiv \epsilon$. Selected function contour and extremal values are marked.

makes it apparent that the GKP codewords are eigenstates of the circuit. Particularly, following the definitions from Ref. [12] we can see $|\bar{0}_{\text{GKP}}\rangle = |0, 0\rangle$ and $|\bar{1}_{\text{GKP}}\rangle = |0, \pi\rangle$. The double-Bloch eigenstates in Eq. (3) satisfy the normalisation $\langle k, \varphi | k', \varphi' \rangle = \delta(k - k')\delta(\varphi - \varphi')$, and the generalised periodic boundary identities $|-1/2, \varphi\rangle = |1/2, \varphi\rangle$ and $|k, -\pi\rangle = e^{-i2\pi k} |k, \pi\rangle$.

A. Perturbative charge and flux noise in the elementary circuit

We include the effect of external voltage and flux noise, as shown in Fig. 1b, with an external gate voltage $V_x(t)$ coupled capacitively via a parasitic capacitor C_x , and an external flux $\Phi_x(t)$ through the circuit loop [16]. In Appendix A, we show that for small C_x the Hamiltonian of the circuit becomes

$$\hat{H}'(t) = -E_Q \cos(2\pi(\hat{n} + n_x(t))) - E_J \cos(\hat{\phi} + \phi_x(t)), \quad (4)$$

where $n_x(t) = C_x V_x(t)/(2e)$ and $\phi_x(t) = 2\pi\Phi_x(t)/\Phi_0$.

For fixed values of the biases, the eigenenergies are $\bar{E}_{k,\varphi}(n_x, \phi_x) = -E_Q \cos(2\pi(k + n_x)) - E_J \cos(\varphi + \phi_x)$. In linear response, the sensitivity of the system to small variation in bias is therefore given by

$$(\partial_{n_x} \bar{E}_{k,\varphi}, \partial_{\phi_x} \bar{E}_{k,\varphi})|_{n_x=\phi_x=0} = \nabla E_{k,\varphi}. \quad (5)$$

For time-dependent noise in the bias parameters, this result implies that the noise sensitivity is determined by $\nabla E_{k,\varphi}$, so that the noise sensitivity vanishes at the critical points, at linear order.

For small-amplitude noise, we expand the Hamiltonian to linear order in the noise terms, so

$$\hat{H}'(t) \simeq \hat{H} + n_x(t)\hat{A}_n + \phi_x(t)\hat{A}_\phi, \quad (6)$$

where

$$\hat{A}_n = 2\pi E_Q \sin(2\pi\hat{n}), \quad (7a)$$

$$\hat{A}_\phi = E_J \sin(\hat{\phi}). \quad (7b)$$

Since $[\hat{H}, \hat{A}_n] = [\hat{H}, \hat{A}_\phi] = 0$, flux and charge noise do not induce transitions between eigenstates. Further, the critical states are null vectors of $\hat{A}_{n,\phi}$, so they are immune to charge and flux noise to first order.

We illustrate the general noise insensitivity using the example of uncorrelated charge and flux noise, for which

$$\langle n_x(t)n_x(t') \rangle = \epsilon_n^2 \delta(t - t'), \quad (8a)$$

$$\langle \phi_x(t)\phi_x(t') \rangle = (2\pi\epsilon_\phi)^2 \delta(t - t'), \quad (8b)$$

$$\langle n_x(t)\phi_x(t') \rangle = 0, \quad (8c)$$

where ϵ_n and ϵ_ϕ are noise amplitudes. With this white noise model, the evolution of the system density matrix, ρ , is given by the master equation [17, 18]

$$\dot{\rho}(t) = -\frac{i}{\hbar}[\hat{H}, \rho(t)] + 2\epsilon_n^2 \mathcal{D}[\hat{A}_n]\rho(t) + 2(2\pi\epsilon_\phi)^2 \mathcal{D}[\hat{A}_\phi]\rho(t), \quad (9)$$

where $\mathcal{D}[A]\rho = A\rho A^\dagger - (\rho A^\dagger A + A^\dagger A\rho)/2$.

To calculate the decoherence rate between superpositions of eigenstates, we suppose that the system is initially in a pure state $|\psi\rangle = \mu|k, \varphi\rangle + \mu'|k', \varphi'\rangle$, so that $\rho(0) = |\psi\rangle\langle\psi|$. Off diagonal elements are right eigenoperators of the lindblad superoperators, but generally with non-zero eigenvalues (i.e., dephasing rates),

$$\mathcal{D}[\hat{A}_n]|k, \varphi\rangle\langle k', \varphi'| = -\frac{1}{2}(2\pi E_Q)^2 \gamma_{2\pi k, 2\pi k'}|k, \varphi\rangle\langle k', \varphi'|,$$

$$\mathcal{D}[\hat{A}_\phi]|k, \varphi\rangle\langle k', \varphi'| = -\frac{1}{2}E_J^2 \gamma_{\varphi, \varphi'}|k, \varphi\rangle\langle k', \varphi'|,$$

where

$$\gamma_{y, y'} = (\sin(y) - \sin(y'))^2. \quad (10)$$

The pure dephasing rate is therefore given by

$$\Gamma_{k,\varphi; k',\varphi'} = (2\pi\epsilon_n E_Q)^2 \gamma_{2\pi k, 2\pi k'} + (2\pi\epsilon_\phi E_J)^2 \gamma_{\varphi, \varphi'}. \quad (11)$$

For any choice of k , there are values of k' for which $\gamma_{2\pi k, 2\pi k'} = 0$, and similarly for φ and φ' . Of particular interest is the fact that for superpositions of the

critical eigenstates both lindblad superoperators vanish, $\gamma_{2\pi k, 2\pi k'} = \gamma_{\varphi, \varphi'} = 0$, so that $\Gamma_{k,\varphi; k',\varphi'} = 0$ when $|k, \varphi\rangle, |k', \varphi'\rangle \in \{|0, 0\rangle, |0, \pi\rangle, |1/2, 0\rangle, |1/2, \pi\rangle\}$. We plot $\Gamma_{0,0; k, \varphi}$ in Figs. 2c and 2d, showing that the dephasing rates from fluctuations in both external bias charge and flux vanish at the critical points. This property makes these states intriguing candidates for robustly storing quantum information.

III. REALISTIC CIRCUIT ELEMENTS

Realistically, the dualmon circuit will have some linear inductance L in the ring, and capacitance C across the JJ [19]. We therefore extend the model to account for the effects of these parasitic elements, and we show that the noise insensitivity of the elementary circuit is retained under certain assumptions for the circuit parameters.

The resulting lumped-element model, shown in Fig. 1c, has an additional circuit node, and the Hamiltonian for the realistic circuit is

$$\hat{\mathcal{H}}_{\text{sys}} = E_C \hat{n}_A^2 + E_L (\hat{\phi}_A - \hat{\phi}_B)^2 - E_Q \cos(2\pi\hat{n}_B) - E_J \cos(\hat{\phi}_A), \quad (12)$$

where $E_C = (2e)^2/(2C)$, $E_L = \Phi_0^2/(8\pi^2 L)$, and the modes labeled A and B refer to the circuit nodes indicated in Fig. 1c. We note that models of this form have been studied in Ref. [20].

A. Energy bands

We assume that L and C are small, so that $E_L, E_C \gg E_Q, E_J$. In this case, the high-frequency dynamics of the associated LC oscillator will dominate, so it is convenient to transform to new conjugate coordinates

$$\hat{\phi}_1 = \hat{\phi}_A - \hat{\phi}_B, \quad \hat{n}_1 = \hat{n}_A, \quad \hat{\phi}_2 = \hat{\phi}_B, \quad \hat{n}_2 = \hat{n}_A + \hat{n}_B. \quad (13)$$

In these coordinates we have

$$\hat{\mathcal{H}}_{\text{sys}} = \hat{H}_{\text{HO}} + \hat{\mathcal{V}}, \quad (14)$$

where

$$\hat{H}_{\text{HO}} = E_C \hat{n}_1^2 + E_L \hat{\phi}_1^2, \quad (15)$$

$$\hat{\mathcal{V}} = -E_Q \cos(2\pi(\hat{n}_1 - \hat{n}_2)) - E_J \cos(\hat{\phi}_1 + \hat{\phi}_2). \quad (16)$$

$\hat{\mathcal{H}}_{\text{sys}}$ commutes with $\cos(2\pi\hat{n}_2)$ and $\cos(\hat{\phi}_2)$, so eigenstates of $\hat{\mathcal{H}}_{\text{sys}}$ will be simultaneous eigenstates of these operators, which are the Zak basis states $|k, \varphi\rangle_2$ ¹. Thus, the eigenstates of $\hat{\mathcal{H}}_{\text{sys}}$ take the form

$$|\Psi_{m; k, \varphi}\rangle_{1,2} = |\psi_m(k, \varphi)\rangle_1 |k, \varphi\rangle_2, \quad (17)$$

¹ Here the subscript $i = 1, 2$ indicates states associated to mode i .

where $|\psi_m(k, \varphi)\rangle_1$ are the eigenstates of the reduced Hamiltonian acting on mode 1,

$$\hat{H}_1(k, \varphi) = \hat{H}_{\text{HO}} + \hat{V}(k, \varphi), \quad (18)$$

with

$$\hat{V}(k, \varphi) = -E_Q \cos(2\pi(\hat{n}_1 - k)) - E_J \cos(\hat{\phi}_1 + \varphi). \quad (19)$$

The eigenenergies $E_{m;k,\varphi}$ of the two-mode Hamiltonian \hat{H}_{sys} , markedly, coincide with those of the mode-1 Hamiltonian $\hat{H}_1(k, \varphi)$.

We are concerned with the limit $E_L, E_C \gg E_Q, E_J$, in which $\hat{H}_1(k, \varphi)$ describes a weakly nonlinear oscillator (i.e., mode 1) that depends parametrically on the quantum numbers k and φ associated to mode 2. We treat $\hat{V}(k, \varphi)$ perturbatively, and so we denote the eigenstates of \hat{H}_{HO} as $|\psi_m^{(0)}\rangle_1$ with eigenenergies $E_m^{(0)} = (m + 1/2)\hbar\Omega$, where

$$\hbar\Omega = 2\sqrt{E_C E_L}. \quad (20)$$

Within the oscillator ground state manifold, $m = 0$, the first order perturbative correction to the energy is

$$\begin{aligned} E_{m=0;k,\varphi}^{(1)} &= {}_1\langle\psi_0^{(0)}|\hat{V}(k, \varphi)|\psi_0^{(0)}\rangle_1 \\ &= -E'_Q \cos(2\pi k) - E'_J \cos(\varphi), \end{aligned} \quad (21)$$

where $E'_Q = e^{-\pi^2/z} E_Q$ and $E'_J = e^{-z/4} E_J$ are renormalised QPS and JJ parameters arising from zero-point motion of mode 1, and $z = \sqrt{E_C/E_L} = \sqrt{L/C} (2e)^2/\hbar$ is a dimensionless oscillator impedance. Equation (21) shows that within the oscillator ground state manifold, mode 2 is governed by the elementary Hamiltonian \hat{H} in Eq. (1), with renormalised QPS and JJ energies. Significantly, the critical points remain at the same locations in the double-Bloch band.

To verify the perturbative arguments above, we numerically solve for $|\psi_m(k, \varphi)\rangle_1$ and eigenenergies $E_{m;k,\varphi}$ non-perturbatively in the Zak basis for mode 1, as described in Appendix B. Figures 3a and 3b show the oscillator ground state manifold energy band $E_{m=0;k,\varphi}$ relative to the unperturbed harmonic oscillator ground state energy, for $E_L, E_C \gg E_Q = E_J$. The nonlinear energies $E_{J,Q}$ are renormalised to $E'_{J,Q}$, but the band structure is otherwise qualitatively the same as the elementary case, and with the same critical eigenstates. We show below that the noise sensitivity vanishes at the critical eigenstates, as for the elementary circuit.

Figures 3c and 3d also demonstrate the first excited manifold, $E_{m=1;k,\varphi}$, relative to the unperturbed harmonic oscillator first excited state energy. In this manifold, the renormalised nonlinear energies are $E''_Q = (1 - 2\pi^2/z)E'_Q$ and $E''_J = (1 - z/2)E'_J$, so that the first excited band may be inverted relative to the ground state manifold (i.e., the locations of minima and maxima are exchanged). It follows that the interband transition energies at the critical points can be made non-degenerate, facilitating spectroscopic addressability of

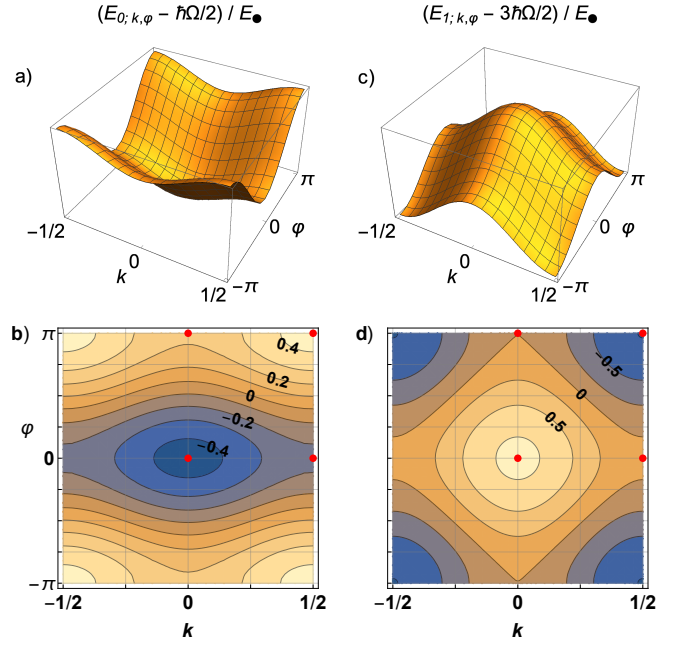


FIG. 3. (a) and (b) The ground state band energy, $E_{m=0;k,\varphi}$, of the realistic dualmon circuit relative to the unperturbed harmonic oscillator ground state energy, $E_{m=0}^{(0)}$. (c) and (d) The first excited state band energy, $E_{m=1;k,\varphi}$. Plots are generated by numerically solving the eigenvalue problem (see Appendix B). On this scale, the difference between the numerical values and the perturbative result in Subsec. III A is less than 0.005 across the band. For illustrative purposes, plots are drawn with $E_Q = E_J \equiv E_{\bullet}$, $E_C/E_J = 200$ and $E_L/E_J = 10$. For these parameter values, $z = \sqrt{20}$, $E'_Q = 0.11E_{\bullet}$, $E'_J = 0.33E_{\bullet}$, $E''_Q = -0.38E_{\bullet}$, and $E''_J = -0.40E_{\bullet}$.

the critical states. This addressability provides an avenue to state preparation: spectroscopic measurements of a given accuracy will localise the system in a narrow range of k and φ near the observed transition energy. This will be discussed in more details in Sec. IV.

B. Perturbative charge and flux noise in the realistic circuit

We introduce charge and flux noise in the same manner as for the elementary circuit [21]. The Hamiltonian is then

$$\begin{aligned} \hat{\mathcal{H}}'_{\text{sys}} &= E_{C_{\Sigma}}(\hat{n}_A + n_x(t))^2 + E_L(\hat{\phi}_A - \hat{\phi}_B - \phi_x(t))^2 \\ &\quad - E_Q \cos(2\pi\hat{n}_B) - E_J \cos(\hat{\phi}_A), \end{aligned} \quad (22)$$

where $E_{C_{\Sigma}} = (2e)^2/(2C_{\Sigma})$ with $C_{\Sigma} = C + C_x$, and n_x and ϕ_x are external bias terms, as discussed earlier. In what follows, we assume that $C_x \ll C$, and take $E_{C_{\Sigma}} = E_C$ for simplicity.

Constant charge and flux bias can be transformed away by suitable gauge choice [22, 23], so we again consider the effect of zero-mean, white noise. As before, we make the

coordinate transformation given by Eq. (13), and expand the Hamiltonian to linear order in the noise terms, so

$$\hat{\mathcal{H}}'_{\text{sys}} \simeq \hat{\mathcal{H}}_{\text{sys}} + n_x(t)\hat{\mathcal{A}}_n + \phi_x(t)\hat{\mathcal{A}}_\phi, \quad (23)$$

where

$$\hat{\mathcal{A}}_n = 2E_C \hat{n}_1, \quad (24a)$$

$$\hat{\mathcal{A}}_\phi = -2E_L \hat{\phi}_1. \quad (24b)$$

The master equation for the noisy system is then

$$\dot{\varrho} = -\frac{i}{\hbar}[\hat{\mathcal{H}}_{\text{sys}}, \varrho] + 2\epsilon_n^2 \mathcal{D}[\hat{\mathcal{A}}_n]\varrho + 2(2\pi\epsilon_\phi)^2 \mathcal{D}[\hat{\mathcal{A}}_\phi]\varrho, \quad (25)$$

where ϱ is the joint density operator for modes 1 and 2.

Since $\hat{\mathcal{A}}_n$ and $\hat{\mathcal{A}}_\phi$ have action on the Hilbert space associated with mode 1 only, they are diagonal within any oscillator manifolds. Using the first order perturbative correction to the oscillator modes, we compute matrix elements of these dissipators in the ground state manifold (see Appendix C for more detail), and find that

$${}_{1,2}\langle \Psi_{0;k,\varphi} | \hat{\mathcal{A}}_n | \Psi_{0;k',\varphi'} \rangle_{1,2} = 2\pi E'_Q \sin(2\pi k) \delta(k-k') \delta(\varphi-\varphi'), \quad (26a)$$

$${}_{1,2}\langle \Psi_{0;k,\varphi} | \hat{\mathcal{A}}_\phi | \Psi_{0;k',\varphi'} \rangle_{1,2} = E'_J \sin(\varphi) \delta(k-k') \delta(\varphi-\varphi'), \quad (26b)$$

which implies

$$\Pi_0 \hat{\mathcal{A}}_n \Pi_0 = 2\pi E'_Q \sin(2\pi \hat{n}_2), \quad (27a)$$

$$\Pi_0 \hat{\mathcal{A}}_\phi \Pi_0 = E'_J \sin(\hat{\phi}_2), \quad (27b)$$

where $\Pi_0 = \int_{-1/2}^{1/2} dk \int_{-\pi}^{\pi} d\varphi |\Psi_{0;k,\varphi}\rangle_{1,2} \langle \Psi_{0;k,\varphi}|$ is the projection onto the ground state manifold. Equations (27a) and (27b) are of the same form as the dissipators for the elementary circuit, Eqs. (7a) and (7b), and so lead to dephasing rates of the same form. That is, a superposition of two eigenstates in the ground state manifold, $\mu |\Psi_{0;k,\varphi}\rangle + \mu' |\Psi_{0;k',\varphi'}\rangle$, will dephase at a rate also given by $\Gamma_{k,\varphi; k',\varphi'}$ in Eq. (11), with the replacements $E_{Q,J} \rightarrow E'_{Q,J}$. As for the elementary circuit, the dephasing rate vanishes for superpositions of the critical states.

C. Parametric and non-perturbative noise sources in the realistic circuit

The Aharonov-Casher interference [24] of phase slips, dependent on charge distribution, could be detrimental to QPS devices. Indeed, phase slips exhibit along a strongly disordered superconducting nanowire [10]; interference of phase slips at different points may cause fluctuations in the phase slip energy E_Q [11, 25], and result in dephasing of coherent superpositions. Phase slip interference on JJ chains (i.e., a granular model of superconducting nanowires [19]) has also been observed experimentally [26], and shown to be a decoherence source in the Josephson-junction-chain based fluxonion qubit

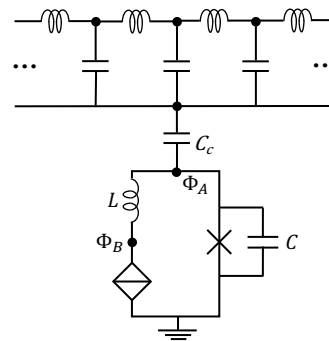


FIG. 4. Lumped-element representation of the capacitive coupling between the realistic dualmon circuit and a waveguide.

[27, 28]. To mitigate such undesirable effect, a possible approach is to fabricate QPS nanowires in the form of short weak links [29, 30], by which phase slips are limited to take place at the narrowest point, thus improving stability of the QPS energy.

The time-dependent charge noise considered in Subsec. III B was perturbative, in which the standard-deviation in the charge was small, $\sigma_{n_x} \ll 1/2$. However, localised, two-level charge traps near the circuit can lead to a random-telegraph charge fluctuation with $\sigma_{n_x} \sim 1/2$, which is no longer perturbative. This gives rise to quantum state diffusion, i.e., shifting of the system state in the charge space. However, as long as the noise magnitude is smaller than one electron worth of charge, we speculate that the errors could be correctable by means of active GKP quantum error correction [12], for which GKP codes were originally designed. A short discussion on specific implementation of such active correction is included in Appendix D.

IV. COUPLING TO A WAVEGUIDE

Realistic devices will need to couple to waveguides with which one can initialise, control, and perform readout on the system. Here we couple the dualmon circuit capacitively to a waveguide and analyse spectroscopy on the device. We then propose a spectroscopic procedure for state preparation.

The waveguide coupling also introduces quantum and thermal noise to the system, so we analyse the additional noise arising from this coupling. As for classical charge and flux noise, we show that superpositions of the critical states are robust with respect to the induced quantum noise, for essentially the same reason, i.e., the band gradient vanishes at the critical points.

A. Transmission spectrum

Figure 4 illustrates a circuit where the dualmon is capacitively coupled to a waveguide. A detailed Hamilto-

nian derivation for this circuit is given in Appendix E. The Hamiltonian for the dualmon system coupled to the waveguide is

$$\hat{\mathcal{H}}_{\text{tot}} = \hat{\mathcal{H}}_{\text{sys}} + \hat{\mathcal{H}}_{\text{wg}} + \hat{\mathcal{H}}_{\text{coup}}, \quad (28)$$

where $\hat{\mathcal{H}}_{\text{sys}}$ is the dualmon Hamiltonian defined in Eq. (14),

$$\hat{\mathcal{H}}_{\text{wg}} = \int d\omega \hbar \omega \hat{a}^\dagger(\omega) \hat{a}(\omega), \quad (29)$$

is the waveguide Hamiltonian describing a continuum of modes, and

$$\hat{\mathcal{H}}_{\text{coup}} = \int d\omega g(\omega) (\hat{a}^\dagger(\omega) + \hat{a}(\omega)) \hat{n}_1, \quad (30)$$

is the interaction with $g(\omega)$ the coupling strength.

We make use of the input-output formalism [31, 32] to calculate the transmission spectrum; relevant calculations are presented in more details in Appendix F. In particular, the dynamics of the dualmon system coupled to the waveguide and driven by a coherent field of amplitude α is governed by

$$\dot{\hat{\rho}} = -\frac{i}{\hbar} [\hat{\mathcal{H}}_{\text{drive}}, \hat{\rho}] + \mathcal{D}[\hat{b}]\hat{\rho}, \quad (31)$$

where

$$\hat{\mathcal{H}}_{\text{drive}} = \hat{\mathcal{H}}_{\text{sys}} - \frac{i\hbar}{2} \sqrt{\gamma} (\alpha e^{-i\omega_D t} \hat{n}_1^+ - \alpha e^{i\omega_D t} \hat{n}_1^-), \quad (32)$$

$$\hat{b} = \sqrt{\gamma} \hat{n}_1^- + \alpha e^{-i\omega_D t} \mathbb{1}. \quad (33)$$

Here \hat{n}_1^+ (\hat{n}_1^-) is the lower (upper) triangularised version of \hat{n}_1 , ω_D is the drive frequency, and $\sqrt{\gamma}$ is proportional to $g(\omega_D)$ determining bandwidth of the spectrum. The transmission is defined as

$$T = |\langle \hat{b} \rangle / \alpha|^2, \quad (34)$$

where $\langle \hat{b} \rangle = \text{Tr}(\hat{b}\hat{\rho})$. We solve the master equation (31), use the obtained results to calculate $\langle \hat{b} \rangle$, and then get the transmission T .

The transmission spectrum assuming the circuit to be initialised in either one of two critical states $|\Psi_{0;k=0,\varphi=0}\rangle_{1,2}$ and $|\Psi_{0;k=0,\varphi=\pi}\rangle_{1,2}$ is displayed in Fig. 5. For illustrative purpose, the transmission has been plotted in dependence on the detuning of the drive frequency ω_D from the transition between the lowest (i.e., ground) and first excited bands for the critical point $(k=0, \varphi=\pi)$, denoted as $\Omega_{0,\pi}^{(1,0)}$ ². It can be seen from Fig. 5 that resonance depends on the system state. This is consistent with the observation made in Subsec. III A, that is, the interband transition frequency is dependent on the state of the device, with the distinguishability of different $|k, \varphi\rangle$ states set by the difference in the interband transition frequency.

² We define $\Omega_{k,\varphi}^{(m,n)} \equiv (E_{m;k,\varphi} - E_{n;k,\varphi})/\hbar$ as the transition frequency from the n^{th} band to the m^{th} band at a fixed pair of (k, φ) .

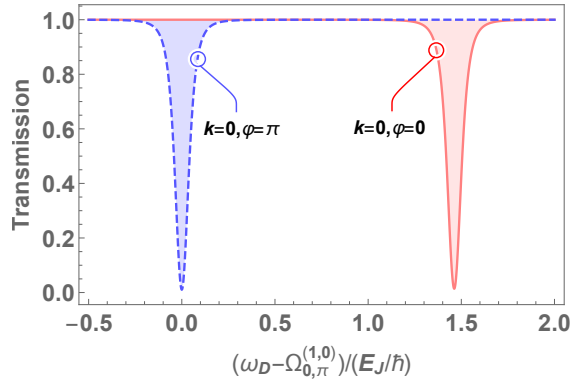


FIG. 5. Transmission spectrum T defined in Eq. (34) with respect to the detuning of the drive frequency ω_D from the transition frequency $\Omega_{0,\pi}^{(1,0)}$ for two critical points, $(k=0, \varphi=0)$ and $(k=0, \varphi=\pi)$. Here $\Omega_{0,\pi}^{(1,0)}$ denotes the interband transition between the ground and first excited bands at the critical point $(k=0, \varphi=\pi)$. Relevant parameters for plotting are chosen as $E_Q = E_J$, $\hbar\Omega = 40\sqrt{5} E_J$, $z = \sqrt{20}$, $\gamma = 0.01 \omega_D$, and $\hbar\alpha^2 = 0.1 E_J$.

B. Qubit initialisation by spectroscopy

The spectroscopic measurement described in the preceding subsection moreover gives a route to state preparation. Since the interband transition frequency between the lowest and first excited bands of the dualmon is (k, φ) -dependent, transmission at a given frequency $\Omega_{k,\varphi}^{(1,0)}$ will localise the system around the corresponding value of (k, φ) ³. As shown in Appendix G scanning over transition frequency is equivalent to scanning over the two biases $n_x \in [-1/2, 1/2]$ and $\phi_x \in [-\pi, \pi)$, one can thus localise the state to some value of (k, φ) starting from a generic state such as a thermal state. Once the value of (k, φ) has been localised, one can adjust (n_x, φ_x) to move the origin of the band in Fig. 3 such that the state becomes localised at any desired point, e.g., the ground state $(k=0, \varphi=0)$.

Choosing, e.g., $(k=0, \varphi=0)$ and $(k=0, \varphi=\pi)$ as the two operating points for the dualmon, logical basis state preparation corresponds to preparing a state highly localised around one of these two values. The exact form of the distributions over (k, φ) is not particularly important, nor is it crucial that the states are pure, as long as they are sufficiently well-localised. This,

³ Note that the mapping between interband frequencies $\Omega_{k,\varphi}^{(1,0)}$ and values of (k, φ) is in general not unique, except for at the ground state $(k=0, \varphi=0)$, and the maximally excited state $(k=1/2, \varphi=\pi)$ (see Fig. 8 in Appendix F). Resolving states with similar transition frequencies can however be done by adjusting n_x and ϕ_x while performing spectroscopy at a given frequency.

perhaps counter intuitive, can be understood by making an analogy with approximate GKP codewords [12]. Two approximate qubit codewords for the dualmon can be defined as

$$|i_L\rangle = \int dk d\varphi \psi_i(k, \varphi) |k, \varphi\rangle, \quad (35)$$

with $\psi_i(k, \varphi)$ some localised distribution around $(k = 0, \varphi = 0)$ for $i = 0$ and $(k = 0, \varphi = \pi)$ for $i = 1$. A well-localised but mixed state can be viewed as an approximate qubit codeword with a set of small (approximately) correctable errors. In other words, we can think of the well-localised mixed state as the codeword $|i_L\rangle$ sent through an error channel with the “size” of the errors bounded by the measurement resolution of the spectroscopic measurement. This is thus analogous to noisy preparation of GKP codewords. In a universal scheme for quantum computing, which we will not discuss here, it is also crucial that the logical operations do not amplify errors too badly, i.e., turning small errors into large ones. Provided that this is true, the two distributions will remain well-localised throughout the computation, and can in principle be distinguished with high fidelity in a final measurement.

We have argued that it should be possible to prepare states well-localised around a single value of (k, φ) using spectroscopic measurements, and furthermore such states can be thought of as imperfect, yet high-quality, qubit codewords. It is however a far more challenging task to prepare superposition states, such as $|+L\rangle = \frac{1}{\sqrt{2}}(|0_L\rangle + |1_L\rangle)$, with a similar guarantee of “small errors”. Preliminary results suggest that introducing symmetry-breaking terms to the Hamiltonian, e.g., breaking the 2π periodicity of $\hat{\phi}_2$, can be used to prepare states of the form $|+L\rangle$. The quality of such operations, as well as the possibility of universal control, will be the subject of future work.

C. Pure dephasing from thermal and quantum noise in the waveguide

The capacitive coupling to the waveguide, in addition to allow performing spectroscopy and state initialisation, opens a channel for noise to appear in the dualmon circuit. The induced noise is manifest via the coupling operator \hat{n}_1 , which is diagonal within each manifold while coupling states among different manifolds. As we are interested in encoding the dualmon in the ground state manifold, say in a superposition of eigenstates $\mu |\Psi_{0;k,\varphi}\rangle_{1,2} + \mu' |\Psi_{0;k',\varphi'}\rangle_{1,2}$, the relevant decoherence source is either pure dephasing within the encoded manifold or transitions to other manifolds. The master equation for the dualmon density operator when considering only pure dephasing in the ground state manifold is [33]

$$\dot{\varrho}_g = -\frac{i}{\hbar} [\hat{\mathcal{H}}_{\text{sys},g}, \varrho_g] + 2\pi \lim_{\omega \rightarrow 0} (J(\omega)(2N(\omega)+1)) \mathcal{D}[\hat{n}_{1,g}] \varrho_g, \quad (36)$$

where ϱ_g , $\hat{\mathcal{H}}_{\text{sys},g}$, and $\hat{n}_{1,g}$ are all projections onto the ground state manifold, $J(\omega) = 1/\hbar^2 \int d\omega' g^2(\omega) \delta(\omega' - \omega)$ is the spectral density, and $N(\omega)$ is the thermal distribution at frequency ω . $\hat{n}_{1,g}$ can be straightforwardly computed from Eqs. (24a) and (27a). The pure dephasing rate of the superposition of interest in the ground state manifold is then found to be

$$\Gamma_{k;k'} = \frac{\pi^2 E'_Q}{E_C} \lim_{\omega \rightarrow 0} (J(\omega)(2N(\omega)+1)) \gamma_{2\pi k, 2\pi k'}, \quad (37)$$

where the function $\gamma_{y,y'}$ has been defined in Eq. (10). In general this is not zero, due to thermal and vacuum fluctuations in the waveguide. However, similar to the case of classical noise in Subsec. III B, we have $\gamma_{2\pi k, 2\pi k'} = 0$ for superpositions of the critical states, so that dephasing from waveguide fluctuations is completely suppressed.

D. Decoherence from thermal waveguide excitation

Another decoherence source stemming from the waveguide coupling is thermal transitions among different manifolds. We show below that provided the harmonic oscillator gap is much larger than $k_B T$ the thermal induced dephasing rate is very small. For this purpose, we express the coupling operator \hat{n}_1 in the form

$$\hat{n}_1 = \int_{-1/2}^{1/2} dl \int_{-\pi}^{\pi} d\theta \sum_{m,n=0}^{\infty} \hat{n}_{1;l,\theta}^{(m,n)}, \quad (38)$$

where $\hat{n}_{1;l,\theta}^{(m,n)} = {}_{1,2}\langle \Psi_{m;l,\theta} | \hat{n}_1 | \Psi_{n;l,\theta} \rangle_{1,2} | \Psi_{m;l,\theta} \rangle_{1,2} \langle \Psi_{n;l,\theta} |$ are eigenoperators of $\hat{\mathcal{H}}_{\text{sys}}$ satisfying the commutation relations $[\hat{\mathcal{H}}_{\text{sys}}, \hat{n}_{1;l,\theta}^{(m,n)}] = \hbar \Omega_{l,\theta}^{(m,n)} \hat{n}_{1;l,\theta}^{(m,n)}$. The master equation for the dualmon density operator, that accounts for the transitions between manifolds, is then given by [33]

$$\begin{aligned} \dot{\varrho} = & -\frac{i}{\hbar} [\hat{\mathcal{H}}_{\text{sys}}, \varrho] \\ & + \iint dld\theta \sum_{m<n} \pi J(\Omega_{l,\theta}^{(n,m)}) (N(\Omega_{l,\theta}^{(n,m)}) + 1) \mathcal{D}[\hat{n}_{1;l,\theta}^{(m,n)}] \varrho \\ & + \iint dld\theta \sum_{m>n} \pi J(\Omega_{l,\theta}^{(m,n)}) N(\Omega_{l,\theta}^{(m,n)}) \mathcal{D}[\hat{n}_{1;l,\theta}^{(m,n)}] \varrho. \end{aligned} \quad (39)$$

In Eq. (39), the second and third lines respectively represent relaxations to lower manifolds and excitations to higher manifolds; notably, the two quantum numbers l and θ are conserved, implying the absence of transitions within each manifold. As well known from the standard two-level-system encoding, either relaxation or excitation dephases coherent superpositions. However, as the dualmon is encoded in superpositions of two eigenstates in the ground state manifold and there are no transitions between these two states, the dephasing rate for the dualmon is determined by excitations out of the ground state manifold only. In Appendix H, we include several calculations comparing dephasing rates

of the ordinary two-level-system encoding and ground-state-manifold one. The relevant dephasing rate, from Eq. (39), is proportional to $J(\Omega_{l,\theta}^{(m>0,0)})N(\Omega_{l,\theta}^{(m>0,0)})$. The waveguide (the bath) is assumed to be in thermal state, i.e., $N(\omega) = 1/(\exp(\hbar\omega/k_B T) - 1)$ and as shown in Appendix E $J(\omega) = \nu\hbar\omega$ with ν a constant, so

$$J(\omega)N(\omega) = \nu\hbar\omega/(\exp(\hbar\omega/k_B T) - 1), \quad (40)$$

which is very small for large $\hbar\omega/k_B T$. Hence, thermal dephasing is very weak as long as $\hbar\Omega_{k,\varphi}^{(1,0)} \gg k_B T$. This condition is inherently satisfied with superconducting circuits, since the working temperature is typically very low.

V. COMPARISONS WITH RELATED SUPERCONDUCTING QUBITS

It is instructive to point out the differences between the proposed circuit and other superconducting qubit devices previously discussed in the literature, namely, the $0 - \pi$ qubit [2–6], the fluxonium [22, 23], and the Aharonov-Casher device [34]. Specifically, the $0 - \pi$ qubit uses two nearly degenerate eigenstates with nearly disjoint support in coordinate space [5], which affords its noise-rejecting properties. Realisation of the $0 - \pi$ qubit would require implementing the π -periodic Josephson junction [2, 3, 35–38]. In comparison, the robustness of the critical states of the dualmon device arises from the fact that the noise operators associated to weak external charge and flux noise commute with the eigenstates suppressing decay, and the gradient of the energy landscape vanishes at the critical states suppressing dephasing.

The lumped circuit of the imperfect fluxonium [22, 23], where phase slip is included at its superinductor [27, 28], is remarkably identical to the realistic dualmon circuit shown in Fig. 1c. However, the essential difference between the two devices lies at the energy scales. In particular, the fluxonium employs a superinductor [22, 23, 39] to make the inductive energy very small; QPS on the superinductor is treated as an undesired noisy source [27]. The JJ present in the fluxonium circuit generally works in the regime of large E_J/E_C . These are in contrast to the dualmon energy scales, which ideally would be $E_L, E_C \gg E_Q, E_J$ (see Subsec. III A). The difference at energy scales then results in the differences in the physics of the two devices. Indeed, fluxon tunneling is the primary process in the fluxonium [27], whereas the dual QPS and JJ elements in the dualmon allow tunneling of both fluxon and Cooper pair. The fluxonium wavefunction in flux space is localised within the wells of the Josephson cosine potential and in charge space is well-localised within a range of a Cooper pair [23]. The dualmon, instead, is completely delocalised in both flux and charge spaces (see Zak states in Eq. (3)). Finally, the Aharonov-Casher device proposed in Ref. [34] is realised basically as a single JJ shunted by a superinductor, and thus closely resembles the fluxonium design;

therefore, the above arguments also hold when comparing such device to the dualmon circuit. Furthermore, in that device the Aharonov-Casher interference effect is utilised to suppress single fluxon tunneling while making pair tunneling dominant. This is different from the dualmon circuit, where only single fluxon tunneling is considered.

We comment briefly on plausible experimental parameters for the dualmon circuit. Josephson and QPS energies can be routinely engineered to be $E_J \sim E_Q \sim h \times 5$ GHz [11, 25, 40, 41]. Parasitic capacitance and self-inductances of order $C \sim 1$ fF and $L \sim 10$ nH are feasible [8, 25, 40] corresponding to parameters for the dualmon circuit of $z \sim 3$ and $\hbar\Omega \sim h \times 50$ GHz $\gg E_J, E_Q$, which is well within the validity range of the approximations employed in this work.

VI. CONCLUSIONS

We have shown that the dualmon circuit, encoded in superpositions of the critical points, is resilient against both classical and quantum white noise. The device nonetheless could suffer from other noise sources, including the charge-dependent Aharonov-Casher effect in QPS devices that lowers the phase slip energy and large temporal charge fluctuations causing diffusion of quantum states. Possibly, the former could be reduced by designing QPS elements in a weak-link form [29, 30], whilst the later might be dealt with via active error correction of the GKP code [12].

Any pair of the critical points could be chosen to represent a qubit; the nearly-degenerate saddle points might be a convenient choice. As discussed qualitatively in Subsec. IV B, state preparation could be performed by interband spectroscopic measurements. The quality with which we can prepare states near the critical points then depends on the spectral resolution of such a measurement.

Relative phase shifts between the critical states may be achieved using tunable JJ and QPS circuit elements, or by using high frequency drive pulses to access excited states of the oscillator mode. Tuning of JJ and QPS energies leaves the critical states unchanged, thus retaining the protected working space of the qubit; introducing tunable elements, however, opens the qubit to new dephasing channels. More general control requires additional symmetry breaking terms in the Hamiltonian. For example, a shunt inductor switched transiently across the JJ breaks the discrete charge translation symmetry of the Hamiltonian, so it will couple the Zak eigenstates of the original circuit. Detailed analysis of control of the state space for one and multiple devices will be the subject of future work.

We conclude that the dualmon circuit considered here offers a promising avenue for robustly storing quantum information, worthy of further study. In particular, it hosts several critical eigenstates, superpositions of which

are insensitive to both charge and flux noise at linear order. This result holds even when the circuit includes parasitic capacitance and inductance. Interestingly, the critical states are physical embodiments of the codewords of the GKP error correcting code. Active fault-tolerant preparation of such states in harmonic oscillators is extremely hard, so the dualmon circuit could possibly offers an alternative path towards accessing these states.

ACKNOWLEDGMENTS

This research was supported by the Australian Research Council Centre of Excellence for Engineered Quantum Systems (EQUS, CE170100009) and a Discovery Early Career Research Award (DE190100380) as well as the Swiss National Science Foundation through the NCCR Quantum Science and Technology. TMS acknowledges visitor support from the Pauli Center for Theoretical Studies, ETH Zurich. We thank J. Cole and V. V. Albert for useful discussions.

Appendix A: Derivation of the biased Hamiltonian, $\hat{H}'(t)$

Here we derive the Hamiltonian $\hat{H}'(t)$ in Eq. (4). Applying the spanning tree model in Ref. [16] for the circuit in Fig. 1b, we choose the fluxes across the QPS and JJ to be $\Phi_Q = \Phi$ and $\Phi_J = \Phi + \Phi_x$, respectively. The Kirchoff current conservation law at the active node of the circuit is

$$\dot{Q}_Q + \dot{Q}_{C_x} + \dot{Q}_J = 0. \quad (\text{A1})$$

From the constitutive laws for circuit elements, we know that the charge that has flowed through the QPS is

$$Q_Q(\dot{\Phi}) \equiv \frac{2e}{2\pi} \arcsin(\dot{\Phi}/V_c), \quad (\text{A2})$$

the charge across the bias capacitor is $Q_{C_x} = C_x(\dot{\Phi} - V_x)$, and the current through the Josephson junction is $\dot{Q}_J \equiv I_J = I_c \sin(2\pi(\Phi + \Phi_x)/\Phi_0)$. We thus find the equation of motion for the circuit is

$$\frac{d}{dt}(Q_Q(\dot{\Phi}) + C_x(\dot{\Phi} - V_x)) + I_c \sin\left(\frac{2\pi}{\Phi_0}(\Phi + \Phi_x)\right) = 0. \quad (\text{A3})$$

We identify terms above with the Euler-Lagrange equation of motion, $\frac{d}{dt}Q - \partial_{\dot{\Phi}}L = 0$ where $Q = \partial_{\dot{\Phi}}L$ is the charge conjugate to $\dot{\Phi}$, which implies

$$Q = \partial L / \partial \dot{\Phi} = Q_Q(\dot{\Phi}) + C_x \dot{\Phi} - Q_x, \quad (\text{A4})$$

$$\partial L / \partial \Phi = -I_c \sin\left(\frac{2\pi}{\Phi_0}(\Phi + \Phi_x)\right), \quad (\text{A5})$$

where $Q_x = C_x V_x$. The Lagrangian is then given by

$$L = \dot{\Phi} Q_Q(\dot{\Phi}) + \frac{2eV_c}{2\pi} \cos\left(\frac{2\pi}{2e} Q_Q(\dot{\Phi})\right) + \frac{C_x}{2} (\dot{\Phi} - V_x)^2 + \frac{I_c \Phi_0}{2\pi} \cos\left(\frac{2\pi}{\Phi_0}(\Phi + \Phi_x)\right). \quad (\text{A6})$$

The Hamiltonian, $H(\Phi, \dot{\Phi}) = \dot{\Phi} Q - L$, is

$$H(\Phi, \dot{\Phi}) = \frac{C_x}{2} \dot{\Phi}^2 - E_Q \cos\left(\frac{2\pi}{2e} Q_Q(\dot{\Phi})\right) - E_J \cos\left(\frac{2\pi}{\Phi_0}(\Phi + \Phi_x)\right), \quad (\text{A7})$$

where $E_Q = 2eV_c/(2\pi)$, $E_J = I_c \Phi_0/(2\pi)$. To compute $H(\Phi, Q)$ we need to invert Eq. (A4) to find $\dot{\Phi} = \dot{\Phi}(Q)$. Implicitly, we have

$$\dot{\Phi} = V_c \sin\left(\frac{2\pi}{2e}(Q - C_x \dot{\Phi} + Q_x)\right). \quad (\text{A8})$$

We cannot solve this analytically for $\dot{\Phi}$, however if $C_x \dot{\Phi} \ll Q$ we expand the right hand-side of Eq. (A8) in powers of C_x , and solve for $\dot{\Phi}$. We find

$$\dot{\Phi} = V_c \sin\left(\frac{2\pi}{2e}(Q + Q_x)\right) \times \left(1 - \frac{2\pi}{2e} C_x V_c \cos\left(\frac{2\pi}{2e}(Q + Q_x)\right)\right) + O(C_x^2). \quad (\text{A9})$$

Substituting this result into Eq. (A7), we obtain

$$H = -E_Q \cos\left(\frac{2\pi}{2e}(Q + Q_x)\right) - E_J \cos\left(\frac{2\pi}{\Phi_0}(\Phi + \Phi_x)\right) + E_{C_x} \cos\left(\frac{4\pi}{2e}(Q + Q_x)\right) + O(C_x^2), \quad (\text{A10})$$

where $E_{C_x} = C_x V_c^2/4$. Quantising the charge and flux operators, and defining $\hat{n} = \hat{Q}/(2e)$ and $\hat{\phi} = 2\pi\hat{\Phi}/\Phi_0$, the Hamiltonian operator is then

$$\hat{H}' = -E_Q \cos(2\pi(\hat{n} + n_x)) - E_J \cos(\hat{\phi} + \phi_x) + E_{C_x} \cos(4\pi(\hat{n} + n_x)), \quad (\text{A11})$$

where $n_x = Q_x/(2e)$ and $\phi_x = 2\pi\Phi_x/\Phi_0$. If the external capacitance is sufficiently small then $E_{C_x} \ll E_Q, E_J$. Since $[\hat{H}, \cos(4\pi(\hat{n} + n_x))] = 0$, this term does not change the eigenstates, and preserves the critical points. We therefore take $E_{C_x} = 0$ for simplicity, yielding Eq. (4).

Appendix B: Eigenvalue problem for mode 1

In the Zak basis, we have the useful operator representations [15, 20]

$$\langle k, \varphi | \hat{n} | \psi \rangle = -i \frac{\partial}{\partial \varphi} \langle k, \varphi | \psi \rangle, \quad (\text{B1})$$

$$\langle k, \varphi | \hat{\phi} | \psi \rangle = \left(-i \frac{\partial}{\partial k} + \varphi\right) \langle k, \varphi | \psi \rangle. \quad (\text{B2})$$

We express eigenstates of the reduced Hamiltonian $\hat{H}_1(k, \varphi)$ in the Zak basis for mode 1, $\{|l, \theta\rangle_1\}$, and we find that $\psi_m(l, \theta; k, \varphi) \equiv {}_1\langle l, \theta | \psi_m(k, \varphi) \rangle_1$ are eigenfunctions of the differential operator

$$H_1(k, \varphi) = E_C \left(-i \frac{\partial}{\partial \theta}\right)^2 + E_L \left(-i \frac{\partial}{\partial l} + \theta\right)^2 - E_J \cos(\theta + \varphi) - E_Q \cos(2\pi(l - k)), \quad (\text{B3})$$

where $\psi_m(l, \theta; k, \varphi)$ satisfies generalised periodic boundary conditions

$$\psi_m(-1/2, \theta; k, \varphi) = \psi_m(1/2, \theta; k, \varphi), \\ \psi_m(l, -\pi; k, \varphi) = e^{2\pi l i} \psi_m(l, \pi; k, \varphi).$$

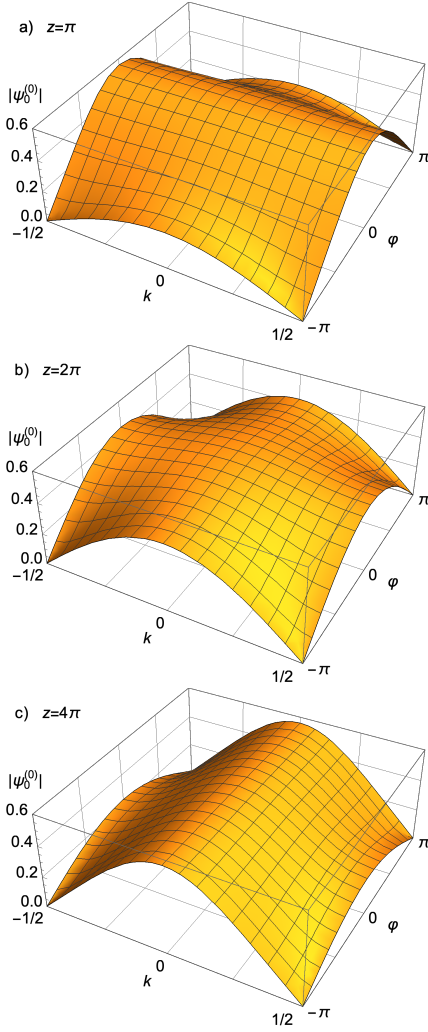


FIG. 6. The harmonic oscillator eigenstates in the Zak basis, $|\langle k, \varphi | \psi_0^{(0)} \rangle|$, for different values of $z = \sqrt{E_C/E_L}$. (a) For $z < 2\pi$, $\psi_0^{(0)}(k, \varphi)$ is somewhat localised in the modular phase (alternatively, the quasi-flux) coordinate, φ , but delocalised in k . (b) For $z = 2\pi$, $\psi_0^{(0)}(k, \varphi)$ is equally delocalised in both coordinates. (c) For $z > 2\pi$, $\psi_0^{(0)}(k, \varphi)$ is somewhat localised in the modular number coordinate (alternatively, the quasi-charge [14]), k , but delocalised in φ .

In this representation, it is straightforward to compute the eigensystem of mode 1 numerically.

It is illustrative to evaluate the well-known LC harmonic oscillator ground states in the Zak basis, \hat{H}_{HO} . In the phase basis, $\psi_0^{(0)}(\phi) = (\pi z)^{-1/4} e^{-\frac{\phi^2}{2z}}$, where $z = \sqrt{E_C/E_L}$. In the Zak basis, we find that

$$\begin{aligned} \psi_0^{(0)}(k, \varphi) &= \sum_{j=-\infty}^{\infty} e^{-2\pi j k i} \psi_0^{(0)}(\varphi - 2\pi j) \\ &= (\pi z)^{-1/4} e^{-\frac{\varphi^2}{2z}} \vartheta_3(\pi k + i\pi\varphi/z, e^{-\frac{2\pi^2}{z}}), \end{aligned} \quad (\text{B4})$$

where $\vartheta_3(u, q) \equiv 1 + 2 \sum_{j=1}^{\infty} q^{j^2} \cos(2uj)$ is an elliptic theta function. The Zak basis highlights the relative lo-

calisation of the ground state in k or φ . We plot this function for $z = \pi, 2\pi$, and 4π in Fig. 6. When the energy scales for the kinetic and potential terms are balanced, at $z = 2\pi$, the ground state is equally delocalised in each coordinate. At this point, the JJ and QPS renormalisation scale factors are equal, i.e., $E'_J/E_J = E'_Q/E_Q$.

Appendix C: Evaluating $\hat{\mathcal{A}}_n$ in the ground state eigenbasis manifold $\{|\Psi_{0;k,\varphi}\rangle_{1,2}\}$

Here we compute ${}_{1,2}\langle \Psi_{0;k,\varphi} | \hat{\mathcal{A}}_n | \Psi_{0;k',\varphi'} \rangle_{1,2}$,

$${}_{1,2}\langle \Psi_{0;k,\varphi} | \hat{\mathcal{A}}_n | \Psi_{0;k',\varphi'} \rangle_{1,2} = 2E_C {}_1\langle \psi_0(k, \varphi) | \hat{n}_1 | \psi_0(k', \varphi') \rangle_1 \times \delta(k - k') \delta(\varphi - \varphi'). \quad (\text{C1})$$

We expand $|\psi_m(k, \varphi)\rangle_1$ to first order in perturbation theory, and for notational convenience we define the matrix element $[[\hat{B}]]_{jm} = {}_1\langle \psi_j^{(0)} | \hat{B} | \psi_m^{(0)} \rangle_1$ for an operator \hat{B} , so

$$|\psi_m(k, \varphi)\rangle_1 = |\psi_m^{(0)}\rangle_1 + \sum_{j \neq m} \frac{[[\hat{V}(k, \varphi)]]_{jm}}{\Delta E_{mj}^{(0)}} |\psi_j^{(0)}\rangle_1, \quad (\text{C2})$$

where $\Delta E_{mj}^{(0)} = E_m^{(0)} - E_j^{(0)} = \hbar\Omega(m - j)$. Then,

$$\begin{aligned} {}_1\langle \psi_0(k, \varphi) | \hat{n}_1 | \psi_0(k, \varphi) \rangle_1 &= \\ [[\hat{n}_1]]_{00} + 2 \sum_{m \neq 0} \text{Re} \left(\frac{[[\hat{n}_1]]_{0m} [[\hat{V}(k, \varphi)]]_{m0}}{\Delta E_{0m}^{(0)}} \right) + O(|\frac{V}{\Delta E}|^2). \end{aligned} \quad (\text{C3})$$

We write the coordinate \hat{n}_1 in terms of creation and annihilation operators \hat{a}_1^\dagger and \hat{a}_1 , i.e., $\hat{n}_1 = i(\hat{a}_1^\dagger - \hat{a}_1)/\sqrt{2z}$. Since \hat{a}_1^\dagger and \hat{a}_1 are off-diagonal in the harmonic oscillator eigenbasis, we find $[[\hat{n}_1]]_{0m} = -i \delta_{m,1}/\sqrt{2z}$. Ignoring terms $O(|\frac{V}{\Delta E}|^2)$ and higher, we find

$${}_1\langle \psi_0(k, \varphi) | \hat{n}_1 | \psi_0(k, \varphi) \rangle_1 = 2 \text{Re} \left(\frac{[[\hat{n}_1]]_{01} [[\hat{V}(k, \varphi)]]_{10}}{\Delta E_{01}^{(0)}} \right). \quad (\text{C4})$$

Evaluating the matrix element for $\hat{V}(k, \varphi)$ gives

$$\begin{aligned} [[\hat{V}(k, \varphi)]]_{10} &= -E_Q {}_1\langle \psi_1^{(0)} | \cos(2\pi(\hat{n}_1 - k)) | \psi_0^{(0)} \rangle_1 \\ &\quad - E_J {}_1\langle \psi_1^{(0)} | \cos(\hat{\phi}_1 + \varphi) | \psi_0^{(0)} \rangle_1, \\ &= -E_Q \int_{-\infty}^{\infty} dn \cos(2\pi(n - k)) \psi_1^{(0)}(n)^* \psi_0^{(0)}(n) \\ &\quad - E_J \int_{-\infty}^{\infty} d\phi \cos(\phi + \varphi) \psi_1^{(0)}(\phi)^* \psi_0^{(0)}(\phi), \\ &= e^{-\frac{\varphi}{z}} \sqrt{\frac{z}{2}} E_J \sin(\varphi) - i\pi e^{-\frac{\pi^2}{z}} \sqrt{\frac{2}{z}} E_Q \sin(2\pi k). \end{aligned}$$

We substitute the results into Eq. (C1), and noting that $\hbar\Omega z = 2E_C$, we obtain Eq. (26a).

The computation for ${}_{1,2}\langle \Psi_{0;k,\varphi} | \hat{\mathcal{A}}_\phi | \Psi_{0;k',\varphi'} \rangle_{1,2}$ is implemented in a similar manner.

Appendix D: Resonator based charge syndrome measurement and qubit readout

We recall that the external charge n_x typically drifts over time, which is a source of noise for the dualmon. It is thus necessary to detect and correct such type of charge noise. A possible way to do so is as follows. Firstly, from Eqs. (23), (27a), and (27b) it follows that one can couple to the system operators

$$\hat{A}'_n = 2\pi E'_Q \sin(2\pi \hat{n}_2), \quad (\text{D1a})$$

$$\hat{A}'_\phi = E'_J \sin(\hat{\phi}_2), \quad (\text{D1b})$$

by capacitively or inductively coupling to the dualmon circuit, respectively. Focusing on an encoding into the ground state $|0,0\rangle$ and one saddle point $|0,\pi\rangle$, the operator \hat{A}'_n can act as syndrome for charge noise. This follows from the fact that a shift in external charge $n_x \rightarrow n_x - \varepsilon$ can equivalently be interpreted as a shift in k . Since $\sin(2\pi \hat{n}_2) |\varepsilon, \varphi\rangle = \sin(2\pi \varepsilon) |\varepsilon, \varphi\rangle$, a shift with magnitude $|\varepsilon| < 1/4$ can in principle be detected by non-destructively measuring \hat{A}'_n .

Also, a measurement of \hat{A}'_ϕ interestingly can be used to readout the logical qubit state. Particularly, we can set the external flux to $\phi_x = -\pi/2$ such that $\hat{A}'_\phi \rightarrow \hat{A}'_{\phi+\pi/2} = E'_J \cos(\hat{\phi}_2)$. As $\cos(\hat{\phi}_2) |0,0\rangle = |0,0\rangle$ and $\cos(\hat{\phi}_2) |0,\pi\rangle = -|0,\pi\rangle$, a measurement of this operator corresponds to a logical basis measurement. Moreover, the \hat{A}'_ϕ -measurement is robust to small shifts in φ .

A potential approach to non-destructively measuring the operators \hat{A}'_n and \hat{A}'_ϕ is to couple the dualmon circuit to a resonator. The resulting coupling is of the similar form to Eq. (23) with the replacements $n_x(t) \rightarrow n_x(t) + \hat{n}_r$, $\phi_x(t) \rightarrow \phi_x(t) + \hat{\phi}_r$, for capacitive or inductive coupling, respectively. Here $\hat{n}_r \sim \hat{a}_r^\dagger + \hat{a}_r$ is the charge bias, and $\hat{\phi}_r \sim i\hat{a}_r^\dagger - i\hat{a}_r$ the flux bias due to the resonator, with \hat{a}_r the resonator annihilation operator. The non-demolition measurement of interest then may be performed by modulating the coupling strength, based on the longitudinal readout scheme proposed in Ref. [42]. A similar scheme might even be employed to enact resonator induced one-qubit and two-qubit phase gates [43]. A more detailed study of resonator based readout and control will be the subject of future work.

Appendix E: Coupling to a waveguide

1. Hamiltonian derivation

Figure 7 shows the microscopic model of the capacitive coupling between the realistic dualmon circuit and the waveguide. The waveguide of length L is discretely decomposed into unit cells of length d . The number of unit cells is $N = L/d$, each of which has an inductance ℓ and a ground capacitance C_w ; the waveguide inductance and capacitance per unit length are $\bar{\ell} = \ell/d$ and $\bar{C}_w = C_w/d$.

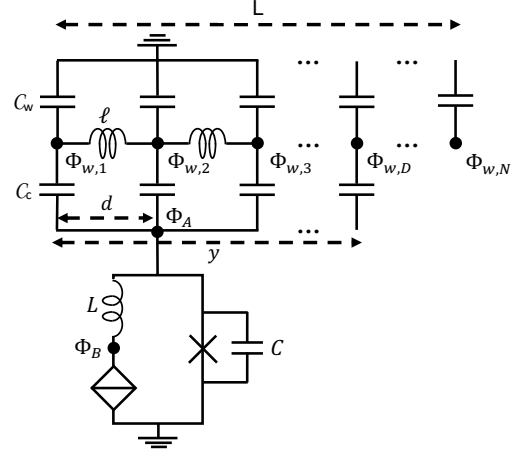


FIG. 7. Microscopic model of the capacitive coupling of the realistic dualmon circuit to the waveguide.

The coupling capacitance is C_c . This capacitance has a length of y across $D = y/d$ unit cells of the waveguide, yielding a distributed coupling capacitance $\bar{C}_c = C_c/D$ per unit cell. We also assume that the size of the coupling capacitance is very small compared to that of the waveguide, i.e., $y \ll L$.

Starting from the classical equations of motion, the Lagrangian of the net circuit is given by

$$\begin{aligned} \mathcal{L}_{\text{tot}} = & \dot{\Phi}_B Q_Q(\dot{\Phi}_B) + \frac{2eV_c}{2\pi} \cos\left(\frac{2\pi}{2e} Q_Q(\dot{\Phi}_B)\right) + \frac{C}{2} \dot{\Phi}_A^2 \\ & + \sum_{j=1}^D \frac{\bar{C}_c}{2} (\dot{\Phi}_{w,j} - \dot{\Phi}_A)^2 + \sum_{j=1}^N \frac{\bar{C}_w}{2} \dot{\Phi}_{w,j}^2 \\ & + \frac{I_c \Phi_0}{2\pi} \cos\left(\frac{2\pi}{\Phi_0} \Phi_A\right) - \frac{1}{2L} (\Phi_A - \Phi_B)^2 \\ & - \sum_{j=1}^N \frac{1}{2\bar{\ell}} (\Phi_{w,j+1} - \Phi_{w,j})^2, \end{aligned} \quad (\text{E1})$$

where

$$Q_Q(\dot{\Phi}_B) = \frac{2e}{2\pi} \arcsin(\dot{\Phi}_B/V_c). \quad (\text{E2})$$

The momenta $Q_A, Q_B, Q_{w,1}, \dots, Q_{w,N}$ are respectively

$$Q_A = C \dot{\Phi}_A + \sum_{j=1}^D \bar{C}_c (\dot{\Phi}_A - \dot{\Phi}_{w,j}), \quad (\text{E3})$$

$$Q_B = Q_Q(\dot{\Phi}_B), \quad (\text{E4})$$

$$Q_{w,j} = \bar{C}_c (\dot{\Phi}_{w,j} - \dot{\Phi}_A) + \bar{C}_w \dot{\Phi}_{w,j}; \quad j = 1, \dots, D, \quad (\text{E5})$$

$$Q_{w,j} = \bar{C}_w \dot{\Phi}_{w,j}; \quad j = D+1, \dots, N. \quad (\text{E6})$$

The Hamiltonian is then

$$\begin{aligned} \mathcal{H}_{\text{tot}} = & -\frac{2eV_c}{2\pi} \cos\left(\frac{2\pi}{2e} Q_Q(\dot{\Phi}_B)\right) - \frac{I_c \Phi_0}{2\pi} \cos\left(\frac{2\pi}{\Phi_0} \Phi_A\right) \\ & + \frac{1}{2L} (\Phi_A - \Phi_B)^2 + \sum_{j=1}^N \frac{1}{2\bar{\ell}} (\Phi_{w,j+1} - \Phi_{w,j})^2 \\ & + \frac{C}{2} \dot{\Phi}_A^2 + \sum_{j=1}^D \frac{\bar{C}_c}{2} (\dot{\Phi}_{w,j} - \dot{\Phi}_A)^2 + \sum_{j=1}^N \frac{\bar{C}_w}{2} \dot{\Phi}_{w,j}^2. \end{aligned} \quad (\text{E7})$$

Eqs. (E4) and (E6) show

$$\dot{\Phi}_B = V_c \sin\left(\frac{2\pi}{2e} Q_B\right), \quad (\text{E8})$$

$$\dot{\Phi}_j = Q_{w,j}/C_w; \quad j = D+1, \dots, N. \quad (\text{E9})$$

Thus, to express \mathcal{H}_{tot} in terms of coordinates and conjugate momenta it requires to find

$$\dot{\Phi}_A = \dot{\Phi}_A(Q_A, Q_{w,1}, \dots, Q_{w,D}), \quad (\text{E10})$$

$$\dot{\Phi}_{w,j} = \dot{\Phi}_{w,j}(Q_A, Q_{w,1}, \dots, Q_{w,D}); \quad j=1, \dots, D, \quad (\text{E11})$$

which, from Eqs. (E3) and (E5), are determined by solving the system of equations

$$\begin{cases} C\dot{\Phi}_A + \sum_{j=1}^D C_c(\dot{\Phi}_A - \dot{\Phi}_{w,j}) = Q_A \\ C_c(\dot{\Phi}_{w,1} - \dot{\Phi}_A) + C_w \dot{\Phi}_{w,1} = Q_{w,1} \\ \vdots \\ C_c(\dot{\Phi}_{w,D} - \dot{\Phi}_A) + C_w \dot{\Phi}_{w,D} = Q_{w,D} \end{cases}. \quad (\text{E12})$$

We substitute the solutions of (E12) (and Eqs. (E8) and (E9) as well) into Eq. (E7), keep terms to first order of C_c only, and get

$$\begin{aligned} \mathcal{H}_{tot} = & -\frac{2eV_c}{2\pi} \cos\left(\frac{2\pi}{2e} Q_B\right) - \frac{I_c \Phi_0}{2\pi} \cos\left(\frac{2\pi}{\Phi_0} \Phi_A\right) \\ & + \frac{1}{2L} (\Phi_A - \Phi_B)^2 + \frac{C - DC_c}{2C^2} Q_A^2 \\ & + \sum_{j=1}^D \frac{C_w - C_c}{2C_w^2} Q_{w,j}^2 + \sum_{j=D+1}^N \frac{1}{2C_w} Q_{w,j}^2 \\ & + \sum_{j=1}^N \frac{1}{2\ell} (\Phi_{w,j+1} - \Phi_{w,j})^2 + \sum_{j=1}^D \frac{C_c}{C_w C} Q_A Q_{w,j}. \end{aligned} \quad (\text{E13})$$

Note that for C_c very small compared to other capacitances, we have $(C - DC_c)/(2C^2) \approx 1/(2C)$ and $(C_w - C_c)/(2C_w^2) \approx 1/(2C_w)$. We then set

$$E_{C_w} = (2e)^2/(2C_w), \quad E_\ell = \Phi_0^2/(8\pi^2 \ell), \quad E_{C_c} = C_c(2e)^2/(C_w C) \\ n_{w,j} = Q_{w,j}/(2e), \quad \phi_{w,j} = 2\pi \Phi_{w,j}/\Phi_0,$$

use notations defined in Appendix A, and change the coordinates of the dualmon circuit as in Eq. (13) to simplify Eq. (E13) into

$$\hat{\mathcal{H}}_{tot} = \hat{\mathcal{H}}_{sys} + \hat{\mathcal{H}}_{wg} + \hat{\mathcal{H}}_{coup}, \quad (\text{E14})$$

where

$$\begin{aligned} \hat{\mathcal{H}}_{sys} = & E_C \hat{n}_1^2 + E_L \hat{\phi}_1^2 \\ & - E_Q \cos(2\pi(\hat{n}_1 - \hat{n}_2)) - E_J \cos(\hat{\phi}_1 + \hat{\phi}_2), \end{aligned} \quad (\text{E15})$$

$$\hat{\mathcal{H}}_{wg} = \sum_{j=1}^N E_{C_w} \hat{n}_{w,j}^2 + E_\ell (\hat{\phi}_{w,j+1} - \hat{\phi}_{w,j})^2, \quad (\text{E16})$$

$$\hat{\mathcal{H}}_{coup} = \sum_{j=1}^D E_{C_c} \hat{n}_1 \hat{n}_{w,j}. \quad (\text{E17})$$

2. Diagonalisation of the waveguide Hamiltonian

We diagonalise the bare Hamiltonian of the waveguide in Eq. (E16). We first define the travelling modes

$$\begin{aligned} \bar{\phi}_s &= \frac{1}{\sqrt{N}} \sum_{j=1}^N e^{-2\pi i j k/N} \hat{\phi}_{w,j} \\ \bar{n}_s &= \frac{1}{\sqrt{N}} \sum_{j=1}^N e^{2\pi i j k/N} \hat{n}_{w,j} \end{aligned}, \quad (\text{E18})$$

which have the inverse

$$\begin{aligned} \hat{\phi}_{w,j} &= \frac{1}{\sqrt{N}} \sum_{k=0}^{N-1} e^{2\pi i j k/N} \bar{\phi}_s \\ \hat{n}_{w,j} &= \frac{1}{\sqrt{N}} \sum_{k=0}^{N-1} e^{-2\pi i j k/N} \bar{n}_s \end{aligned}. \quad (\text{E19})$$

By this, Eq. (E16) becomes

$$\hat{\mathcal{H}}_{wg} = 2 \sum_{k=0}^{N/2-1} E_{C_w} \bar{n}_s \bar{n}_{N-s} + 2E_\ell (1 - \cos(\frac{2\pi k}{N})) \bar{\phi}_s \bar{\phi}_{N-s}. \quad (\text{E20})$$

We then introduce symmetric and antisymmetric modes

$$\begin{aligned} \tilde{n}_{s,+} &= (\bar{n}_s + \bar{n}_{N-s})/\sqrt{2} \\ \tilde{n}_{s,-} &= i(\bar{n}_s - \bar{n}_{N-s})/\sqrt{2} \\ \tilde{\phi}_{s,+} &= (\bar{\phi}_s + \bar{\phi}_{N-s})/\sqrt{2} \\ \tilde{\phi}_{s,-} &= -i(\bar{\phi}_s - \bar{\phi}_{N-s})/\sqrt{2} \end{aligned}, \quad (\text{E21})$$

where $0 < k < N/2 - 1$. It follows that

$$\begin{aligned} \hat{\mathcal{H}}_{wg} = & \sum_{s=0}^{N/2-1} E_{C_w} (\tilde{n}_{s,+}^2 + \tilde{n}_{s,-}^2) \\ & + 2E_\ell (1 - \cos \frac{2\pi s}{N}) (\tilde{\phi}_{s,+}^2 + \tilde{\phi}_{s,-}^2). \end{aligned} \quad (\text{E22})$$

We define

$$\begin{aligned} \tilde{n}_{s,\pm} &= \left(\frac{2E_\ell(1 - \cos 2\pi s/N)}{E_{C_w}}\right)^{1/4} \tilde{\tilde{n}}_{s,\pm} \\ \tilde{\phi}_{s,\pm} &= \left(\frac{E_{C_w}}{2E_\ell(1 - \cos 2\pi s/N)}\right)^{1/4} \tilde{\tilde{\phi}}_{s,\pm} \\ \hat{a}_{s,\pm} &= (-i\tilde{\tilde{\phi}}_{s,\pm} + \tilde{\tilde{n}}_{s,\pm})/\sqrt{2} \\ \hat{a}_{s,\pm}^\dagger &= (i\tilde{\tilde{\phi}}_{s,\pm} + \tilde{\tilde{n}}_{s,\pm})/\sqrt{2} \\ \hbar\omega_s &= \sqrt{2E_{C_w} E_\ell (1 - \cos(2\pi s/N))} \end{aligned}, \quad (\text{E23})$$

and take the limit $N \rightarrow \infty$ to achieve

$$\omega_s = \pi s / (L\sqrt{\bar{C}_w \bar{\ell}}), \quad (\text{E24})$$

$$\hat{\mathcal{H}}_{wg} = \sum_{s=0}^{\infty} \hbar\omega_s (\hat{a}_{s,+}^\dagger + \hat{a}_{s,+} + \hat{a}_{s,-}^\dagger - \hat{a}_{s,-}). \quad (\text{E25})$$

3. The coupling Hamiltonian

We rewrite the coupling Hamiltonian (E17) in terms of $\hat{a}_{s,\pm}$ and $\hat{a}_{s,\pm}^\dagger$. Concretely,

$$\begin{aligned}
\hat{\mathcal{H}}_{\text{coup}} &= \sum_{j=1}^D E_{C_c} \hat{n}_1 \hat{n}_{w,j} \\
&= \sum_{j=1}^D E_{C_c} \hat{n}_1 \frac{1}{\sqrt{N}} \sum_{s=0}^{N-1} e^{-2\pi i j s/N} \tilde{n}_s \\
&= \sum_{j=1}^D E_{C_c} \hat{n}_1 \frac{1}{\sqrt{N}} \sum_{s=1}^{N/2-1} (e^{-2\pi i j s/N} \tilde{n}_s + e^{2\pi i j s/N} \tilde{n}_{N-s}) \\
&= \sum_{j=1}^D E_{C_c} \hat{n}_1 \frac{1}{\sqrt{N}} \sum_{s=1}^{N/2-1} (e^{-2\pi i j s/N} (\tilde{n}_{s,+} - i \tilde{n}_{s,-})/\sqrt{2} + e^{2\pi i j s/N} (\tilde{n}_{s,+} + i \tilde{n}_{s,-})/\sqrt{2}) \\
&= \sum_{j=1}^D E_{C_c} \hat{n}_1 \sqrt{\frac{2}{N}} \sum_{s=1}^{N/2-1} (\cos(2\pi j s/N) \tilde{n}_{s,+} - \sin(2\pi j s/N) \tilde{n}_{s,-}) \\
&= E_{C_c} \hat{n}_1 \sqrt{\frac{2}{N}} \sum_{s=1}^{N/2-1} \int_0^y \frac{dx}{d} (\cos(2\pi s x/L) \tilde{n}_{s,+} - \sin(2\pi s x/L) \tilde{n}_{s,-}) \quad (x = jd) \\
&= E_{C_c} \hat{n}_1 \sqrt{\frac{2}{N}} \sum_{s=1}^{N/2-1} \left(\frac{1}{2\pi s d} \sin(2\pi s y/L) \tilde{n}_{s,+} - \frac{1}{\pi s d} \sin^2(\pi s y/L) \tilde{n}_{s,-} \right) \\
&= E_{C_c} \hat{n}_1 \sqrt{\frac{2}{N}} \sum_{s=1}^{N/2-1} \left(\frac{y}{d} \tilde{n}_{s,+} - \frac{\pi s y^2}{dL} \tilde{n}_{s,-} \right) \quad (\text{the second term will be dropped in the limit } L \rightarrow \infty) \\
&= \frac{C_c (2e)^2}{C_w C} \hat{n}_1 \sqrt{\frac{2}{N}} \sum_{s=1}^{N/2-1} \tilde{n}_{s,+} \quad (\text{note that } E_{C_c} = C_c (2e)^2 / (C_w C) \text{ and } C_c y/d = C_c D = C_c) \\
&= \frac{C_c (2e)^2}{C_w C} \hat{n}_1 \sqrt{\frac{2}{N}} \sum_{s=1}^{N/2-1} \left(\frac{2E_\ell (1 - \cos(2\pi s/N))}{E_{C_w}} \right)^{1/4} \tilde{n}_{s,+} \\
&= \frac{C_c (2e)^2}{C_w C} \hat{n}_1 \sqrt{\frac{2}{N}} \sum_{s=1}^{N/2-1} \left(\frac{4E_\ell (\pi s d/L)^2}{E_{C_w}} \right)^{1/4} \tilde{n}_{s,+} \\
&= \frac{C_c (2e)^2}{C_w C} \hat{n}_1 \sqrt{\frac{2}{L}} \sum_{s=1}^{N/2-1} \left(\frac{E_\ell}{E_{C_w}} \right)^{1/4} \left(\frac{2\pi s}{L} \right)^{1/2} \tilde{n}_{s,+} \\
&= \sum_{s=0}^{\infty} g_s (\hat{a}_{s,+}^\dagger + \hat{a}_{s,+}) \hat{n}_1, \tag{E26}
\end{aligned}$$

where

$$g_s = (2eC_c/C) \sqrt{2\hbar\omega_s/(\bar{C}_w L)}. \tag{E27}$$

Since $\hat{\mathcal{H}}_{\text{coup}}$ couples only modes $(s, +)$ of the waveguide to the dualmon system, in the expression of $\hat{\mathcal{H}}_{\text{wg}}$ in Eq. (E25) we can ignore modes $(s, -)$. For brevity we further shorten the subscript $(s, +)$ into s , yielding

$$\hat{\mathcal{H}}_{\text{wg}} = \sum_s \hbar\omega_s \hat{a}_s^\dagger \hat{a}_s, \tag{E28}$$

$$\hat{\mathcal{H}}_{\text{coup}} = \sum_s g_s (\hat{a}_s^\dagger + \hat{a}_s) \hat{n}_1. \tag{E29}$$

Taking the continuum limit [44], the two above Hamiltonians become

$$\hat{\mathcal{H}}_{\text{wg}} = \int_{-\infty}^{\infty} d\omega \hbar\omega \hat{a}^\dagger(\omega) \hat{a}(\omega), \tag{E30}$$

$$\hat{\mathcal{H}}_{\text{coup}} = \int_{-\infty}^{\infty} d\omega g(\omega) (\hat{a}^\dagger(\omega) + \hat{a}(\omega)) \hat{n}_1, \tag{E31}$$

where the lower limit of the frequency ω has been extended to $-\infty$ [31], and

$$g(\omega) = (2eC_c/C) \sqrt{2\hbar\omega Z_{\text{wg}}/\pi}, \tag{E32}$$

with $Z_{\text{wg}} = \sqrt{\ell/\bar{C}_w}$ the waveguide impedance. The spectral density is given by

$$J(\omega) = \frac{1}{\hbar^2} \int_{-\infty}^{\infty} d\omega g^2(\omega) \delta(\omega - \omega_s) = \frac{8e^2}{\pi\hbar} \frac{C_c^2}{C^2} Z_{\text{wg}} \omega. \tag{E33}$$

We can write $J(\omega) = \nu\hbar\omega$ with

$$\nu = \frac{8e^2}{\pi\hbar^2} \frac{C_c^2}{C^2} Z_{\text{wg}}. \tag{E34}$$

Appendix F: Input-output calculations

We employ the rotating wave approximation and the Markov approximation [31, 32] to simplify the coupling Hamiltonian in Eq. (E31) to

$$\hat{\mathcal{H}}_{\text{coup}} = \int_{-\infty}^{\infty} d\omega \hbar \sqrt{\gamma/2\pi} (\hat{a}^\dagger(\omega) \hat{n}_1^- + \hat{a}(\omega) \hat{n}_1^+), \tag{F1}$$

where $\hbar \sqrt{\gamma/2\pi} \equiv g(\omega_D)$ is the coupling strength evaluated at the drive frequency ω_D , and \hat{n}_1^\pm (\hat{n}_1^-) is the lower (upper) triangularised version of \hat{n}_1 . Note that the Markov approximation is valid in the regime of narrowband interaction, and the operator \hat{n}_1^\pm in terms of the

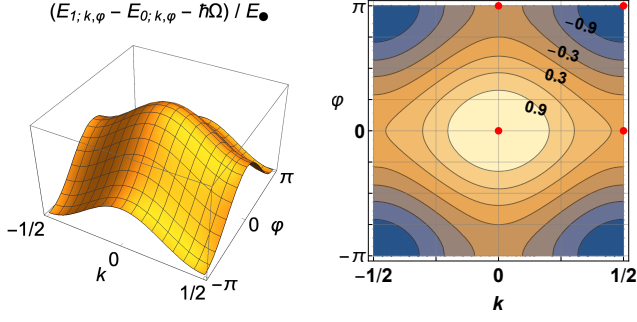


FIG. 8. (Left) and (Right) Three-dimensional and contour plots of the transition frequency between the the ground state and first excited state manifolds relative to the unperturbed harmonic oscillator frequency, $\hbar\Omega_{k,\varphi}^{(1,0)} - \hbar\Omega \equiv E_{1;k,\varphi} - E_{0;k,\varphi} - \hbar\Omega$. The transition at the ground state ($k = 0, \varphi = 0$) and the maximally excited state ($k = 1/2, \varphi = \pi$) is unique, i.e., maximal and minimal respectively, whereas the transition at each saddle point is degenerate. For illustrative purposes, plots are drawn with $E_Q = E_J \equiv E_{\bullet}$, $E_C/E_J = 200$ and $E_L/E_J = 10$.

eigenbasis $\{|\Psi_{m;k,\varphi}\rangle_{1,2}\}$ is of the form

$$\hat{n}_1^\dagger = \sum_{m>n} \int_{-1/2}^{1/2} \int_{-\pi}^{\pi} dk d\varphi_{1,2} \langle \Psi_{m;k,\varphi} | \hat{n}_1 | \Psi_{n;k,\varphi} \rangle_{1,2} \times |\Psi_{m;k,\varphi}\rangle_{1,2} \langle \Psi_{n;k,\varphi} |. \quad (\text{F2})$$

The master equation for the system density operator and the input-output relation are then, using the results in Refs. [31, 32], given by Eqs. (31) - (33) in the main text.

The spectrum displayed in Fig. 5 is obtained by assuming the dualmon state initially in the ground state manifold with a specific pair of (k, φ) , say, the state $|\Psi_{0;k,\varphi}\rangle_{1,2}$. We then approximate the dualmon as a two-level system with eigensystem

$$\begin{aligned} |\Psi_{0;k,\varphi}\rangle_{1,2}; & E_{0;k,\varphi} = \hbar\Omega/2 - E'_Q \cos(2\pi k) - E'_J \cos(\varphi) \\ |\Psi_{1;k,\varphi}\rangle_{1,2}; & E_{1;k,\varphi} = 3\hbar\Omega/2 - E''_Q \cos(2\pi k) - E''_J \cos(\varphi), \end{aligned}$$

where

$$\begin{aligned} E'_Q &= e^{-\pi^2/z} E_Q \\ E'_J &= e^{-z/4} E_J \\ E''_Q &= (1 - 2\pi^2/z) E'_Q \\ E''_J &= (1 - z/2) E'_J \end{aligned} \quad (\text{F3})$$

The transition frequency, $\hbar\Omega_{k,\varphi}^{(1,0)} = E_{1;k,\varphi} - E_{0;k,\varphi}$, is

$$\hbar\Omega_{k,\varphi}^{(1,0)} = \hbar\Omega + \frac{2\pi^2}{z} E'_Q \cos(2\pi k) + \frac{z}{2} E'_J \cos(\varphi). \quad (\text{F4})$$

In Fig. 8, we plot the variation of $\Omega_{k,\varphi}^{(1,0)}$ with respect to (k, φ) . The transition is unique at the ground state ($k = 0, \varphi = 0$) and the maximally excited state ($k = 1/2, \varphi = \pi$) only, being maximal and minimal respectively.

We move to the frame rotating at the drive frequency ω_D , making the master equation (31) time-independent.

We then solve for the steady-state solution of this master equation, and compute the transmission. Relevant parameters for plotting are chosen as $E_Q = E_J, \hbar\Omega = 40\sqrt{5} E_J, z = \sqrt{20}, \gamma = 0.01 \omega_D$, and $\hbar\alpha^2 = 0.1 E_J$. Noteworthy, a time-dependent treatment with higher truncation for the transmission problem yields a considerably similar result.

Appendix G: Scanning over bias charge and flux

We recall that the spectrum shown in Fig. 3 is computed by numerically solving the eigensystem of mode 1 described by the Hamiltonian $\hat{H}_1(k, \varphi)$ in Eq. (18) in the absence of flux and charge biases. When the two biases are nonzero, the Hamiltonian of mode 1 is

$$\begin{aligned} \hat{H}_1(k, \varphi; n_x, \phi_x) &= E_C (\hat{n}_1 + n_x)^2 + E_L (\hat{\phi}_1 - \phi_x)^2 \\ &\quad - E_Q \cos(2\pi(\hat{n}_1 - k)) - E_J \cos(\phi_1 + \varphi). \end{aligned} \quad (\text{G1})$$

It can be checked that under the unitary transformation

$$\hat{U}(n_x, \phi_x) = \exp(i\hat{n}_1 \phi_x) \exp(i\hat{\phi}_1 n_x), \quad (\text{G2})$$

$\hat{H}_1(k, \varphi; n_x, \phi_x)$ becomes

$$\hat{U}(n_x, \phi_x) \hat{H}_1(k, \varphi; n_x, \phi_x) \hat{U}^\dagger(n_x, \phi_x) = \hat{H}_1(k + n_x, \varphi + \phi_x). \quad (\text{G3})$$

This implies the spectrum of $\hat{H}_1(k, \varphi; n_x, \phi_x)$ is obtained by shifting the origin of the $\hat{H}_1(k, \varphi)$ -spectrum to $(-n_x, -\phi_x)$. After turning on the bias parameters the system state (initially assumed to be an eigenstate) is changed into a new eigenstate with a new eigenenergy and new transition frequencies. Hence, scanning over the biases $n_x \in [-1/2, 1/2]$ and $\phi_x \in [-\pi, \pi]$ maps the full spectrum of the dualmon system.

Appendix H: Thermal induced dephasing rate

We calculate the dephasing rates due to thermal excitations and relaxations for two different cases, that is, a qubit that is encoded in an ordinary two-level system, and a qubit that is encoded in the ground state manifold analogous to the proposed dualmon qubit.

The master equation for the standard two-level-system case is

$$\dot{\rho} = -\frac{i}{\hbar} [\hat{H}, \rho] + \gamma_- \mathcal{D}[\hat{\sigma}_-] \rho + \gamma_+ \mathcal{D}[\hat{\sigma}_+] \rho, \quad (\text{H1})$$

where

$$\begin{aligned} \hat{H} &= \frac{1}{2} \hbar\omega (|e\rangle \langle e| - |g\rangle \langle g|) \\ \hat{\sigma}_- &= |g\rangle \langle e| \\ \hat{\sigma}_+ &= |e\rangle \langle g| \end{aligned}, \quad (\text{H2})$$

and $\gamma_- (\gamma_+)$ is the relaxation (excitation) rate. From the master equation, we find the evolution equation for the off-diagonal element ρ_{eg} as follows

$$\dot{\rho}_{eg} = -i\omega \rho_{eg} - \frac{1}{2} (\gamma_+ + \gamma_-) \rho_{eg}, \quad (\text{H3})$$

showing the dephasing rate is proportional to the sum of both the relaxation and excitation rates.

With regards to the qubit encoded in the ground state manifold as in the dualmon device, we assume the system possesses a ground state manifold consisting of $|g_1\rangle$ and $|g_2\rangle$ and an excited state manifold with $|e_1\rangle$ and $|e_2\rangle$. By analogy to the coupling operator \hat{n}_1 in Subsec. IV D, we further assume that the coupling of the system to a heat bath does not induce transitions within each manifold, but allows selected transitions between different manifolds, namely, $|g_j\rangle \leftrightarrow |e_j\rangle$ (not including $|g_j\rangle \leftrightarrow |e_{j'}\rangle$ for $j \neq j'$). In this case, the relevant master equation is

$$\dot{\rho} = -\frac{i}{\hbar}[\hat{\mathcal{H}}, \rho] + \sum_{j=1}^2 \left(\gamma_-^{(j)} \mathcal{D}[\hat{\sigma}_-^{(j)}] \rho + \gamma_+^{(j)} \mathcal{D}[\hat{\sigma}_+^{(j)}] \rho \right), \quad (\text{H4})$$

where

$$\begin{aligned} \hat{\mathcal{H}} &= \sum_{j=1}^2 \frac{1}{2} \hbar \omega_j (|e_j\rangle \langle e_j| - |g_j\rangle \langle g_j|) \\ \hat{\sigma}_-^{(j)} &= |g_j\rangle \langle e_j| \\ \hat{\sigma}_+^{(j)} &= |e_j\rangle \langle g_j| \end{aligned}, \quad (\text{H5})$$

and $\gamma_-^{(j)}$ and $\gamma_+^{(j)}$ are respectively the relaxation and excitation rates between $|g_j\rangle$ and $|e_j\rangle$. The time evolution for the off-diagonal element $\rho_{g_1 g_2}$, which is related to dephasing of the dualmon qubit, is then

$$\dot{\rho}_{g_1 g_2} = \frac{1}{2} i (\omega_1 - \omega_2) \rho_{g_1 g_2} - \frac{1}{2} (\gamma_+^{(1)} + \gamma_+^{(2)}) \rho_{g_1 g_2}. \quad (\text{H6})$$

This result demonstrates that the dephasing rate for the dualmon qubit is determined by the excitation rates out of the ground state manifold only, remarkably differing from the standard two-level-system case.

-
- [1] P. Bonderson and C. Nayak, Phys. Rev. B **87**, 195451 (2013).
- [2] A. Kitaev, arXiv:cond-mat/0609441 (2006).
- [3] P. Brooks, A. Kitaev, and J. Preskill, Phys. Rev. A **87**, 052306 (2013).
- [4] J. M. Dempster, B. Fu, D. G. Ferguson, D. I. Schuster, and J. Koch, Phys. Rev. B **90**, 094518 (2014).
- [5] P. Groszkowski, A. Di Paolo, A. Grimsmo, A. Blais, D. Schuster, A. Houck, and J. Koch, New J. Phys. **20**, 043053 (2018).
- [6] A. D. Paolo, A. L. Grimsmo, P. Groszkowski, J. Koch, and A. Blais, New J. Phys. **21**, 043002 (2019).
- [7] J. M. Martinis, M. H. Devoret, and J. Clarke, Phys. Rev. B **35**, 4682 (1987).
- [8] J. Mooij and C. Harmans, New J. Phys. **7**, 219 (2005).
- [9] J. Mooij and Y. V. Nazarov, Nat. Phys. **2**, 169 (2006).
- [10] O. V. Astafiev, L. B. Ioffe, S. Kafanov, Y. A. Pashkin, K. Y. Arutyunov, D. Shahar, O. Cohen, and J. S. Tsai, Nature **484**, 355 (2012).
- [11] S. E. de Graaf, S. T. Skacel, T. Hönigl-Decrinis, R. Shaikhaidarov, H. Rotzinger, S. Linzen, M. Ziegler, U. Hübner, H. G. Meyer, V. Antonov, E. Il'ichev, A. V. Ustinov, A. Y. Tzalenchuk, and O. V. Astafiev, Nat. Phys. **14**, 590 (2018).
- [12] D. Gottesman, A. Kitaev, and J. Preskill, Phys. Rev. A **64**, 012310 (2001).
- [13] B. C. Travaglione and G. J. Milburn, Phys. Rev. A **66**, 052322 (2002).
- [14] K. Likharev and A. Zorin, J. Low Temp. Phys. **59**, 347 (1985).
- [15] J. Zak, Phys. Rev. Lett. **19**, 1385 (1967).
- [16] M. H. Devoret, *Quantum fluctuations in electrical circuits* (Edition de Physique, France, 1997).
- [17] A. A. Budini, Phys. Rev. A **64**, 052110 (2001).
- [18] T. M. Stace and C. H. W. Barnes, Phys. Rev. A **65**, 062308 (2002).
- [19] K. A. Matveev, A. I. Larkin, and L. I. Glazman, Phys. Rev. Lett. **89**, 096802 (2002).
- [20] S. Ganeshan and M. Levin, Phys. Rev. B **93**, 075118 (2016).
- [21] X. You, J. A. Sauls, and J. Koch, Phys. Rev. B **99**, 174512 (2019).
- [22] J. Koch, V. Manucharyan, M. H. Devoret, and L. I. Glazman, Phys. Rev. Lett. **103**, 217004 (2009).
- [23] V. E. Manucharyan, J. Koch, L. I. Glazman, and M. H. Devoret, Science **326**, 113 (2009).
- [24] Y. Aharonov and A. Casher, Phys. Rev. Lett. **53**, 319 (1984).
- [25] J. T. Peltonen, O. V. Astafiev, Y. P. Korneeva, B. M. Voronov, A. A. Korneev, I. M. Charaev, A. V. Semenov, G. N. Golt'sman, L. B. Ioffe, T. M. Klapwijk, and J. S. Tsai, Phys. Rev. B **88**, 220506 (2013).
- [26] I. M. Pop, B. Douçot, L. Ioffe, I. Protopopov, F. Lecocq, I. Matei, O. Buisson, and W. Guichard, Phys. Rev. B **85**, 094503 (2012).
- [27] V. E. Manucharyan, N. A. Masluk, A. Kamal, J. Koch, L. I. Glazman, and M. H. Devoret, Phys. Rev. B **85**, 024521 (2012).
- [28] N. A. Masluk, I. M. Pop, A. Kamal, Z. K. Mineev, and M. H. Devoret, Phys. Rev. Lett. **109**, 137002 (2012).
- [29] M. Vanević and Y. V. Nazarov, Phys. Rev. Lett. **108**, 187002 (2012).
- [30] J. T. Peltonen, Z. H. Peng, Y. P. Korneeva, B. M. Voronov, A. A. Korneev, A. V. Semenov, G. N. Golt'sman, J. S. Tsai, and O. V. Astafiev, Phys. Rev. B **94**, 180508 (2016).
- [31] C. Gardiner and M. Collett, Phys. Rev. A **31**, 3761 (1985).
- [32] J. Combes, J. Kerckhoff, and M. Sarovar, Adv. Phys. X **2**, 784 (2017).
- [33] H. P. Breuer and F. Petruccione, *The theory of open quantum systems* (Oxford University Press, Great Clarendon Street, 2002).
- [34] M. T. Bell, W. Zhang, L. B. Ioffe, and M. E. Gershenson, Phys. Rev. Lett. **116**, 107002 (2016).
- [35] S. Gladchenko, D. Olaya, E. Dupont-Ferrier, B. Douçot, L. B. Ioffe, and M. E. Gershenson, Nat. Phys. **5**, 48 (2009).
- [36] B. Douçot and L. B. Ioffe, Rep. Prog. Phys. **75**, 072001 (2012).
- [37] M. T. Bell, J. Paramanandam, L. B. Ioffe, and M. E. Gershenson, Phys. Rev. Lett. **112**, 167001 (2014).

- [38] W. Smith, A. Kou, X. Xiao, U. Vool, and M. Devoret, arXiv:1905.01206 (2019).
- [39] T. M. Hazard, A. Gyenis, A. Di Paolo, A. T. Asfaw, S. A. Lyon, A. Blais, and A. A. Houck, Phys. Rev. Lett. **122**, 010504 (2019).
- [40] V. Bouchiat, D. Vion, P. Joyez, D. Esteve, and M. Devoret, Phys. Scr. **1998**, 165 (1998).
- [41] N. G. N. Constantino, M. S. Anwar, O. W. Kennedy, M. Dang, P. A. Warburton, and J. C. Fenton, Nanomaterials **8**, 442 (2018).
- [42] N. Didier, J. Bourassa, and A. Blais, Phys. Rev. Lett. **115**, 203601 (2015).
- [43] B. Royer, A. L. Grimsmo, N. Didier, and A. Blais, Quantum **1**, 11 (2017).
- [44] S. Fan, Ş. E. Kocabaş, and J.-T. Shen, Phys. Rev. A **82**, 063821 (2010).